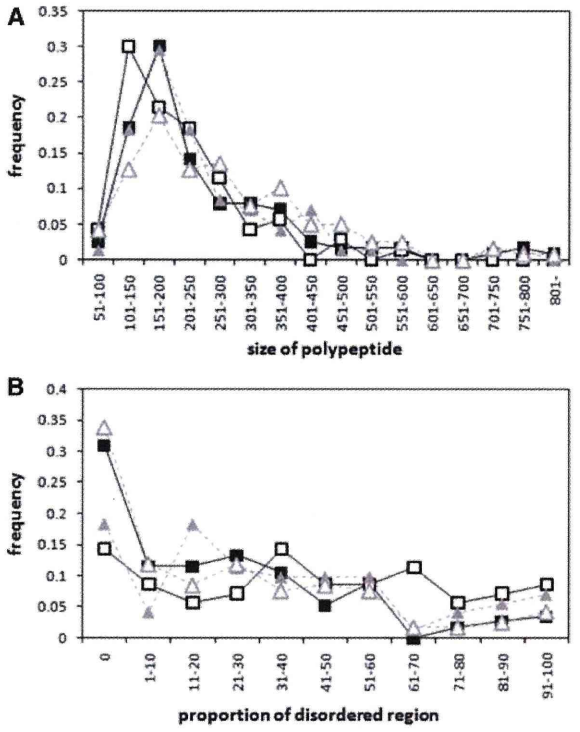

Fig. 3 Distribution of (A) polypeptide sizes and (B) disordered regions in data set_ME. The black squares and grey triangles signify protein expression and solubility, respectively. The filled symbols represent positive data, whereas the open symbols show negative data. The horizontal and vertical axis, respectively show the size and the frequency of the polypeptides.

effect on protein expression. Although it has been suggested that the codon usage influences protein expression (*25–27*), little correlation between rare codons and protein expression was detected in this study. The discrepancy might be explained by the fact that the data set does not include point mutation experiments that change low-usage codons into high-usage ones. Therefore, the estimation suggests the possibility that the influence of rare codons cannot be evaluated. In addition, many selected features are corresponding to amino acids that are encoded by several codons. These observations are the same as those reported by Welch *et al.* (*28*).

Regarding the amino acid information, in the *in vivo E. coli* expression system, the number of features that passed the Student's *t*-test is larger for protein solubility than for protein expression. Particularly, there were many features related to protein solubility in the C-terminal region. Charged residues have a positive effect on both protein expression and solubility, but aromatic residues have a negative effect. In addition, a sulfur-containing residue influences only the protein solubility. In the wheat germ cell-free expression system, the number of selected features is smaller than that in the *in vivo E. coli* expression system. Specifically, the presence of the charged and sulfur-containing residues has little effect on protein solubility. Non-polar residues show the opposite effect in the *in vivo E. coli* expression system.

Regarding the structural information, in the *in vivo E. coli* expression system, the number of features that passed the Student's *t*-test is larger for protein expression than for protein solubility. Statistical analyses revealed that the difficulty of expressing a protein tends to increase in the presence of more disordered regions (Fig. 3B). In contrast, the secondary structure has no effect on protein expression/solubility.

In the wheat germ cell-free expression system, the number of structural features that passed the Student's *t*-test is smaller than that in the *in vivo E. coli* expression system, along with the number of sequence features. In this study, we also examined the correlation between the protein expression/solubility and the number of folded domains predicted by DOMpro (*29*). No significant relation was found (data not shown). This is because more than half of the proteins in our data set have multiple domains, and it is difficult to estimate the number of domains from amino acid information. For that reason, our data set might be unsuitable for analyzing the relation between the number of domains and the protein expression/solubility.

In this study, the definition of the terminal region was 60 nt. To lend credence to the analysis, we estimated the important parameters using new definitions of the terminal region, 30 and 90 nt, and compared them. A strong relationship between protein expression and the presence of rare-frequency codons was not detected in the *in vivo E. coli* expression system, although the some of codons having statistically significant difference changed depending on the length of the terminal region. For the amino acid information, similar features passed the Student's *t*-test. Overall, the results indicated that the tendencies of the important features were the same under any conditions (Supplementary Fig. S1).

Generality of the features

To assess the generality of the features selected in the previous section, we built statistical models that classified the overexpressed proteins and the soluble proteins, based on the sequence information. Then, we compared the classification abilities of the two models produced from the different data sets.

In the *in vivo E. coli* expression system, using data set_ME, the statistical models' abilities were estimated using a 5-fold cross validation test (Table II). The accuracies, which signified the proportions of correct prediction, were 77.6 and 71.4%, respectively, for protein expression and solubility in the *in vivo E. coli* expression system. These values were almost identical to those of the models using all features, presented in the 'Materials and Methods' section. Next, we built a statistical model trained using data set_ME, and evaluated its classification ability using data set_SE (Table II). Based on the accuracy (*Acc.*), the classification ability for data set_SE was slightly lower than that for data set_ME. This difference in the ability between the two models is considered to reflect the experimental error that data set_SE includes, because it was much smaller than the experimental error rate inferred from the analysis of data set_ME. Therefore, the two kinds

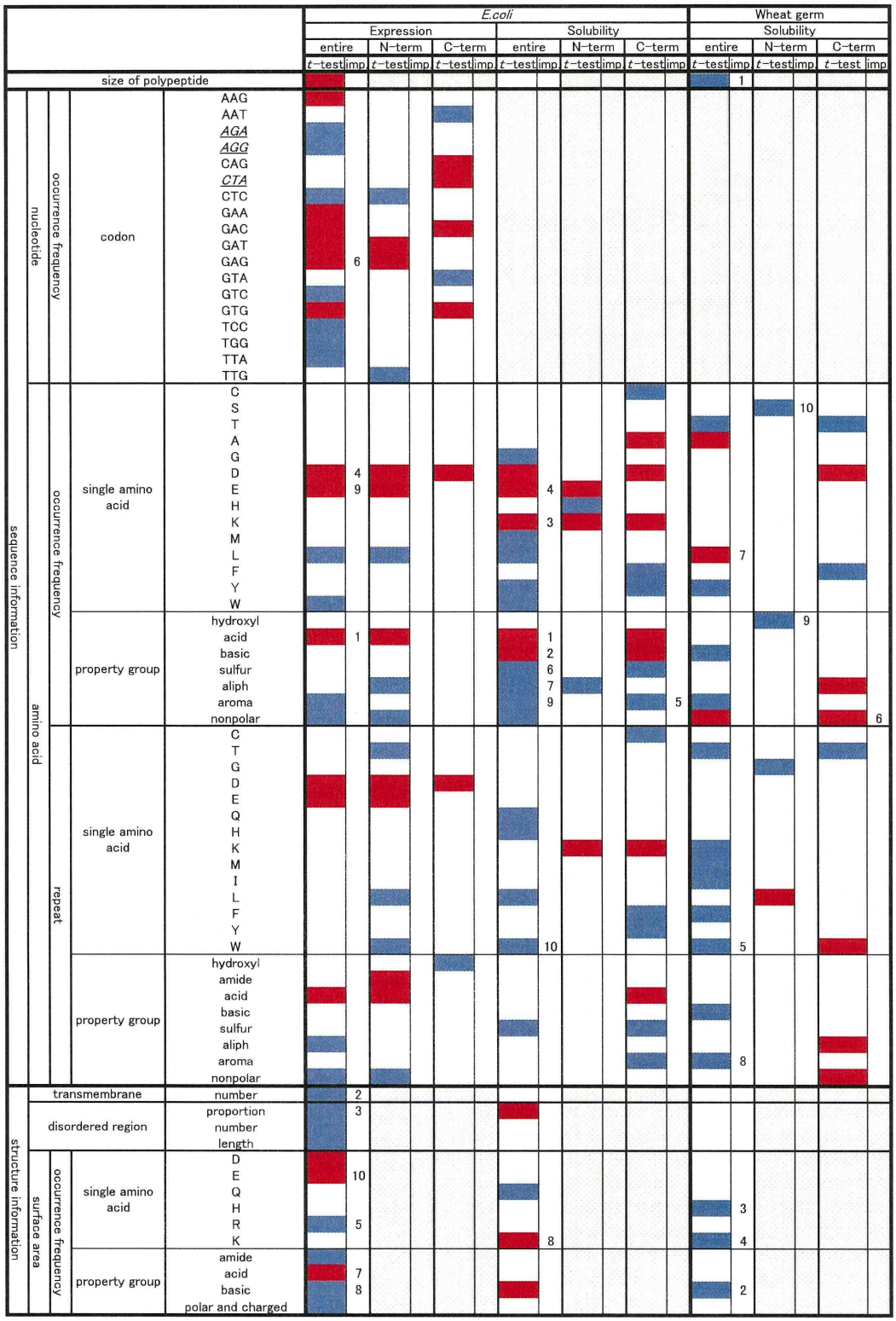

Fig. 4 Comparison of features associated with protein expression/solubility in the two expression systems. Only the features with statistically significant differences detected by the Student's *t*-test are listed in this figure. *t*-test shows the results of the Student's *t*-test. Red signifies the features that have a positive effect on protein expression or solubility, and blue shows the features that have a negative influence. White denotes features not found to have a statistically significant difference; grey shows that no statistical test was done. Entire, N-term, and C-term signify features computed using the entire chain, the N-terminal region, and the C-terminal region, respectively. 'imp.' shows the ranking of features that contribute to protein expression/solubility. The ranking was determined for three categories: protein expression in the *in vivo E. coli*, protein solubility in the *in vivo E. coli*, and protein solubility in wheat germ. The rare-frequency codons in the genetic code of *E. coli* are italicized and underlined.

Table II. Classification abilities of protein expression/solubility in the two expression systems.

		Expression			Solubility		
Expression system	Data set	Recall	Precision	*Acc.*	Recall	Precision	*Acc.*
Escherichia coli	Data set_ME	0.807	0.838	0.776	0.673 (0.296)	0.468 (0.429)	0.714 (0.587)
	Data set_SE	0.876	0.702	0.694	0.424 (0.295)	0.551 (0.432)	0.671 (0.610)
Wheat Germ	Data set_MW	–	–	–	0.736 (0.302)	0.853 (0.897)	0.714 (0.537)
	Data set_SW	–	–	–	0.892 (0.294)	0.718 (0.846)	0.682 (0.469)

The prediction results were classified into four categories: TP is the number of true positives, which is defined as the number of correctly predicted positives. Similarly, FP, TN and FT denote the numbers of false positives, which are defined, respectively, as: negatives that were incorrectly predicted as positives, the number of true negatives, which are defined as correctly predicted negatives, and the number of false negatives, which are defined as positives incorrectly predicted as negatives. Recall and Precision were defined as [=TP/(TP + FP)] and [=TP/(TP + FN)], respectively. *Acc.* [=(TP + TN)/(TP + TN + FP + FN)] represents the proportion of correctly identified positives plus negatives. A hyphen shows that no statistical test was done. The figures in parentheses signify the results of Wilkinson and Harrison model.

of statistical models are considered to have comparable classification abilities. A similar tendency was observed for the wheat germ cell-free expression system (Table II).

These results indicate that the characteristics of the two pairs of data sets—data set_ME and data set_SE, and data set_MW and data set_SW—are similar. Consequently, the features selected in the previous section represent the general characteristics of the protein expression/solubility in each expression system. Therefore, these features in each expression system are considered to be the minimal sets of features associated with protein expression/solubility.

The RF model can estimate the importance of features more simply than commonly-used machine learning methods, such as support vector machine (SVM) (*30*). We estimated the 10 important features based on the mean degrees of *Acc.* (Fig. 4). A comparison of the two expression systems revealed that the key features associated with protein solubility are different. The features related to charge occupied the top rank in the *in vivo E. coli* expression system, while they are hardly found in the wheat germ cell-free expression system.

Discussion

We identified a minimal set of features associated with protein expression/solubility in two expression systems, by the application of two statistical analyses. A comparison of the features associated with protein expression/solubility in the *in vivo E. coli* expression system revealed their different influences. In short, the 'structural information' has a strong influence at the protein expression stage, whereas the amino acid 'sequence information' exerts effects at the protein solubility stage (Fig. 4). These observations suggest a mechanism for yielding a soluble protein in the *in vivo E. coli* expression system. Regarding the protein expression stage, increased numbers of disordered regions and transmembrane regions act to prevent protein expression. Experiments with individual proteins have also shown that disordered regions affect protein expression (*31*). In addition, the presence of charged residues on the protein surface has a positive effect on protein expression. These are common characteristics of globular proteins. For this reason, it may be important for a protein to fold into the proper structure at the protein expression stage. In contrast, the amino acid sequence information is important for the solubility stage. The statistical analysis indicated that an abundance of charged residues in the C-terminal region leads increase of protein solubility. In a study of an individual protein, Kato *et al.* (*32*) reported that adding several arginine residues to the C-terminus of BPTI increased its solubility by preventing aggregation. Therefore, it may be important for a protein not to aggregate at the protein solubility stage.

A comparison of the two expression systems revealed two important points. One is that the number of features associated with protein solubility in the wheat germ cell-free expression system is smaller than that in the *in vivo E. coli* expression system (Fig. 4). This observation implies that the wheat germ cell-free expression system is less sensitive to the various sequence and structural features of a protein, corresponding to the fact that the wheat germ cell-free expression system has a higher success rate than the *in vivo E. coli* expression system in generating soluble proteins (Table I). The other is that the key features in the two expression systems are different. In the *in vivo E. coli* expression system, the charge is important, but it has little influence on the solubility in the wheat germ cell-free expression system. The differences between the features in the two expression systems might be related to the translation speed (*33*). In general, the speed is faster in bacteria than in eukaryotes. The charged residues are considered to be important for partial fording in the *in vivo E. coli* expression system.

The minimal sets of features associated with protein expression/solubility in the two expression systems are useful to screen targets in protein expression experiments. When the statistical model that used the minimal set of features identified in this study was compared with Wilkinson's statistical model (*11*) to predict the *in vitro* solubility of a recombinant protein in an *E. coli* expression system, the *Acc.* of our model for data set_SE was 6.1% higher than that of Wilkinson's model.

Supplementary Data

Supplementary Data are available at *JB* Online.

Acknowledgements

We thank the members of the molecular function team at the Computational Biology Research Center (CBRC) and Dr Kuroda at Tokyo University of Agriculture and Technology (TUAT) for helpful discussions and advice.

Funding

The Okawa Foundation for Information and Telecommunications.

Conflict of interest

None declared.

References

1. Clark, E.D.B. (1998) Refolding of recombinant proteins. *Curr. Opin. Biotechnol.* **9**, 157–163
2. Doray, B., Chen, C.D., and Kemper, B. (2001) N-terminal deletions and His-tag fusions dramatically affect expression of cytochrome p450 2C2 in bacteria. *Arch. Biochem. Biophys.* **393**, 143–153
3. Sati, S.P., Singh, S.K., Kumar, N., and Sharma, A. (2002) Extra terminal residues have a profound effect on the folding and solubility of a Plasmodium falciparum sexual stage-specific protein over-expressed in *Escherichia coli*. *Eur. J. Biochem.* **269**, 5259–5263
4. Kapust, R.B. and Waugh, D.S. (1999) *Escherichia coli* maltose-binding protein is uncommonly effective at promoting the solubility of polypeptides to which it is fused. *Protein Sci.* **8**, 1668–1674
5. Tresaugues, L., Collinet, B., Minard, P., Henckes, G., Aufrere, R., Blondeau, K., Liger, D., Zhou, C.Z., Janin, J., Van Tilbeurgh, H., and Quevillon-Cheruel, S. (2004) Refolding strategies from inclusion bodies in a structural genomics project. *J. Struct. Funct. Genomics* **5**, 195–204
6. Andersen, D.C. and Krummen, L. (2002) Recombinant protein expression for therapeutic applications. *Curr. Opin. Biotechnol.* **13**, 117–123
7. Kramer, G., Kudlicki, W., Hardesty, B., Higgens, S.J., and Hames, B.D. (1999) Cell-free coupled transcription-translation systems from *Escherichia coli*. In *Protein Expression: A Practical Approach* (Higgens, S.J. and Hames, B.D., eds.), pp. 201–223, Oxford University Press, Oxford
8. Clemens, M.M., Prujin, G.J., Higgens, S.J., and Hames, B.D. (1999) Protein synthesis in eukaryotic cell-free systems. In *Protein Expression. A Practical Approach* (Higgens, S.J. and Hames, B.D., eds.), pp. 129–165, Oxford University Press, Oxford
9. Goshima, N., Kawamura, Y., Fukumoto, A., Miura, A., Honma, R., Satoh, R., Wakamatsu, A., Yamamoto, J., Kimura, K., Nishikawa, T., Andoh, T., Iida, Y., Ishikawa, K., Ito, E., Kagawa, N., Kaminaga, C., Kanehori, K., Kawakami, B., Kenmochi, K., Kimura, R., Kobayashi, M., Kuroita, T., Kuwayama, H., Maruyama, Y., Matsuo, K., Minami, K., Mitsubori, M., Mori, M., Morishita, R., Murase, A., Nishikawa, A., Nishikawa, S., Okamoto, T., Sakagami, N., Sakamoto, Y., Sasaki, Y., Seki, T., Sono, S., Sugiyama, A., Sumiya, T., Takayama, T., Takayama, Y., Takeda, H., Togashi, T., Yahata, K., Yamada, H., Yanagisawa, Y., Endo, Y., Imamoto, F., Kisu, Y., Tanaka, S., Isogai, T., Imai, J., Watanabe, S., and Nomura, N. (2008) Human protein factory for converting the transcriptome into an in vitro-expressed proteome. *Nat. Methods* **5**, 1011–1017
10. He, M. (2008) Cell-free protein synthesis: applications in proteomics and biotechnology. *N. Biotechnol.* **25**, 126–132
11. Wilkinson, D.L. and Harrison, R.G. (1991) Predicting the solubility of recombinant proteins in *Escherichia coli*. *Biotechnology* **9**, 443–448
12. Christendat, D., Yee, A., Dharamsi, A., Kluger, Y., Savchenko, A., Cort, J.R., Booth, V., Mackereth, C.D., Saridakis, V., Ekiel, I., Kozlov, G., Maxwell, K.L., Wu, N., McIntosh, L.P., Gehring, K., Kennedy, M.A., Davidson, A.R., Pai, E. F., Gerstein, M., Edwards, A.M., and Arrowsmith, C.H. (2000) Structural proteomics of an archaeon. *Nat. Struct. Biol.* **7**, 903–909
13. Bertone, P., Kluger, Y., Lan, N., Zheng, D., Christendat, D., Yee, A., Edwards, A.M., Arrowsmith, C.H., Montelione, G.T., and Gerstein, M. (2001) SPINE: an integrated tracking database and data mining approach for identifying feasible targets in high-throughput structural proteomics. *Nucleic Acids Res.* **29**, 2884–2898
14. Goh, C.S., Lan, N., Douglas, S.M., Wu, B., Echols, N., Smith, A., Milburn, D., Montelione, G.T., Zhao, H., and Gerstein, M. (2004) Mining the structural genomics pipeline: identification of protein properties that affect high-throughput experimental analysis. *J. Mol. Biol.* **336**, 115–130
15. Luan, C.H., Qiu, S., Finley, J.B., Carson, M., Gray, R.J., Huang, W., Johnson, D., Tsao, J., Reboul, J., Vaglio, P., Hill, D.E., Vidal, M., Delucas, L.J., and Luo, M. (2004) High-throughput expression of *C. elegans* proteins. *Genome Res.* **14**, 2102–2010
16. Idicula-Thomas, S. and Balaji, P.V. (2005) Understanding the relationship between the primary structure of proteins and its propensity to be soluble on overexpression in *Escherichia coli*. *Protein Sci.* **14**, 582–592
17. Niwa, T., Ying, B.W., Saito, K., Jin, W., Takada, S., Ueda, T., and Taguchi, H. (2009) Bimodal protein solubility distribution revealed by an aggregation analysis of the entire ensemble of *Escherichia coli* proteins. *Proc. Natl Acad. Sci. USA* **106**, 4201–4206
18. Maruyama, Y., Wakamatsu, A., Kawamura, Y., Kimura, K., Yamamoto, J., Nishikawa, T., Kisu, Y., Sugano, S., Goshima, N., Isogai, T., and Nomura, N. (2009) Human Gene and Protein Database (HGPD): a novel database presenting a large quantity of experiment-based results in human proteomics. *Nucleic Acids Res.* **37**, 762–766
19. Li, W. and Godzik, A. (2006) Cd-hit: a fast program for clustering and comparing large sets of protein or nucleotide sequences. *Bioinformatics* **22**, 1658–1659
20. Rost, B. (1996) PHD: predicting one-dimensional protein structure by profile-based neural networks. *Methods Enzymol.* **266**, 525–539
21. Krogh, A., Larsson, B., von Heijne, G., and Sonnhammer, E.L. (2001) Predicting transmembrane protein topology with a hidden Markov model: application to complete genomes. *J. Mol. Biol.* **305**, 567–580
22. Hirose, S., Shimizu, K., Kanai, S., Kuroda, Y., and Noguchi, T. (2007) POODLE-L: a two-level SVM prediction system for reliably predicting long disordered regions. *Bioinformatics* **23**, 2046–2053
23. Ahmad, S., Gromiha, M.M., and Sarai, A. (2003) RVP-net: online prediction of real valued accessible surface area of proteins from single sequences. *Bioinformatics* **19**, 1849–1851

24. Liaw, A. and Wiener, M. (2002) Classification and Regression by randomForest. *R News* **2**, 18–22
25. Makrides, S.C. (1996) Strategies for achieving high-level expression of genes in *Escherichia coli*. *Microbiol. Rev.* **60**, 512–538
26. Drummond, D.A. and Wilke, C.O. (2008) Mistranslation-induced protein misfolding as a dominant constraint on coding-sequence evolution. *Cell* **134**, 341–352
27. Lorimer, D., Raymond, A., Walchli, J., Mixon, M., Barrow, A., Wallace, E., Grice, R., Burgin, A., and Stewart, L. (2009) Gene composer: database software for protein construct design, codon engineering, and gene synthesis. *BMC Biotechnol.* **9**, 36
28. Welch, M., Govindarajan, S., Ness, J.E., Villalobos, A., Gurney, A., Minshull, J., and Gustafsson, C. (2009) Design parameters to control synthetic gene expression in *Escherichia coli*. *PLoS One* **4**, e7002
29. Cheng, J., Sweredoski, M., and Baldi, P. (2006) DOMpro: protein domain prediction using profiles, secondary structure relative solvent accessibility, and recursive neural network. *Data Min. Knowl. Disc.* **13**, 1–10
30. Breinman, L. (2001) Random forests. *Mach. Learn.* **45**, 5–32
31. Quevillon-Cheruel, S., Leulliot, N., Gentils, L., van Tilbeurgh, H., and Poupon, A. (2007) Production and crystallization of protein domains: how useful are disorder predictions? *Curr. Protein Pept. Sci.* **8**, 151–160
32. Kato, A., Maki, K., Ebina, T., Kuwajima, K., Soda, K., and Kuroda, Y. (2007) Mutational analysis of protein solubility enhancement using short peptide tags. *Biopolymers* **85**, 12–18
33. Siller, E., DeZwaan, D.C., Anderson, J.F., Freeman, B.C., and Barral, J.M. (2010) Slowing bacterial translation speed enhances eukaryotic protein folding efficiency. *J. Mol. Biol.* **396**, 1310–1318

JOURNAL OF NATURAL PRODUCTS

Note

pubs.acs.org/jnp

Trichostatin Analogues JBIR-109, JBIR-110, and JBIR-111 from the Marine Sponge-Derived *Streptomyces* sp. RM72

Takahiro Hosoya,[†] Takatsugu Hirokawa,[‡] Motoki Takagi,*[,†] and Kazuo Shin-ya*[,§]

[†]Biomedicinal Information Research Center (BIRC), Japan Biological Informatics Consortium (JBIC), 2-4-7 Aomi, Koto-ku, Tokyo 135-0064, Japan

[‡]Computational Biology Research Center (CBRC), National Institute of Advanced Industrial Science and Technology (AIST), 2-4-7 Aomi, Koto-ku, Tokyo 135-0064, Japan

[§]Biomedicinal Information Research Center (BIRC), National Institute of Advanced Industrial Science and Technology (AIST), 2-4-7 Aomi, Koto-ku, Tokyo 135-0064, Japan

Supporting Information

ABSTRACT: Three new trichostatin analogues, JBIR-109 (**1**), JBIR-110 (**2**), and JBIR-111 (**3**), were isolated from the culture of the marine sponge-derived *Streptomyces* sp. strain RM72, together with trichostatin A (**4**) and trichostatic acid (**5**). The planar structures of **1**−**3** were determined on the basis of extensive NMR and MS analyses. In addition, the absolute configurations of the amino acid residues were determined by Marfey's method. The histone deacetylase inhibitory activities of **1**−**5** were examined, and their structure−activity relationships are discussed.

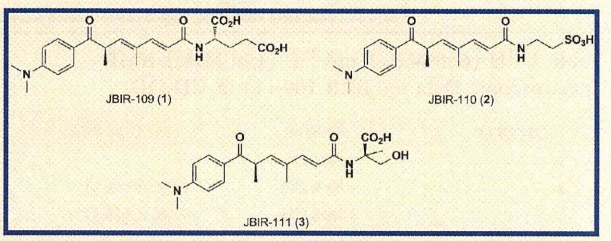

Histone deacetylases (HDACs) play an important role in the epigenetic regulation of gene expression by catalyzing the deacetylation of lysine residues in histone proteins, stimulating chromatin condensation, and promoting transcriptional repression.[1,2] Human HDACs are divided into five classes/subclasses on the basis of their homology to yeast HDACs: class I (HDAC1, 2, 3, and 8), class IIa (HDAC4, 5, 7, and 9), class IIb (HDAC6 and 10), class III (SIRT1, 2, 3, 4, 5, 6, and 7), and class IV (HDAC11). Because aberrant epigenetic changes are hallmarks of cancer, HDACs are promising targets for the development of anticancer drugs. Inhibitors of HDACs can induce cell-cycle arrest, differentiation, and tumor cell death. In fact, several HDAC inhibitors are currently in clinical trials for the treatment of both solid and hematologic malignancies.[1,2]

In our search for HDAC inhibitors, we isolated a novel trichostatin analogue, JBIR-17, in which a serine residue is attached to C-1 of trichostatic acid via an amide bond, from the culture of *Streptomyces* sp. 26634.[3] Upon further screening, we discovered three additional trichostatin analogues, JBIR-109 (**1**), JBIR-110 (**2**), and JBIR-111 (**3**), from the culture of *Streptomyces* sp. RM72, which was associated with a marine sponge collected from a mesopelagic area. We report herein the isolation, structure elucidation, and biological activities of **1**−**3**.

Streptomyces sp. RM72 was cultured in production medium with 50% artificial seawater. Compounds **1**−**3**, together with trichostatin A (**4**)[4] and trichostatic acid (**5**),[5] were recovered from the culture supernatant by using HP-20 resin, followed by purification with sequential chromatography utilizing MPLC and HPLC.

The structures of **1**−**3** were primarily elucidated by spectroscopic analyses. The presence of an amide functional group was suggested by an IR absorption at 1650 cm^{-1}. The UV absorption maxima at 340 and 264 nm, together with ^{1}H and ^{13}C NMR data for **1**−**3** (Table 1 and Table S1), suggested that the basic structural skeletons were identical to that of **5**. Detailed structural information was obtained from the HSQC, HMBC, and DQF-COSY spectra of **1**−**3** (Figure 1).

The molecular formula of **1** was established as $C_{22}H_{28}N_2O_6$ on the basis of HRESIMS data ($[M + H]^+$; *m/z*, 417.2029). In addition to the trichostatic acid portion of the structure, the sequence from the α-methine proton H-2′ (δ_H 4.50; δ_C 53.5) to methylene protons H-4′ (δ_H 2.40) through methylene protons H-3′ (δ_H 1.98, 2.20) was observed. HMBC correlations between H-3′ and two carboxylic carbonyl carbons, C-1′ (δ_C 175.3) and C-5′ (δ_C 176.5), suggested a glutamic acid moiety. Finally, HMBC correlations between both the olefinic proton H-2 and the α-methine proton H-2′ and an amide carbonyl carbon C-1 (δ_C 169.0) established the structure of **1** as a glutamate-substituted trichostatic acid.

The molecular formulas of **2** and **3** were determined to be $C_{19}H_{26}N_2O_5S$ and $C_{21}H_{28}N_2O_5$ on the basis of the HRESIMS data ($[M + H]^+$, *m/z* 395.1655 and $[M + H]^+$, *m/z* 389.2067), respectively. The trichostatic acid core structure in **2** and **3** was established on the basis of NMR data similarly to that described for **1**. For **2**, a COSY correlation between the amino methylene protons H-1′ (δ_H 3.67, δ_C 36.7) and methylene protons H-2′

Received: October 17, 2011
Published: January 25, 2012

Chart 1

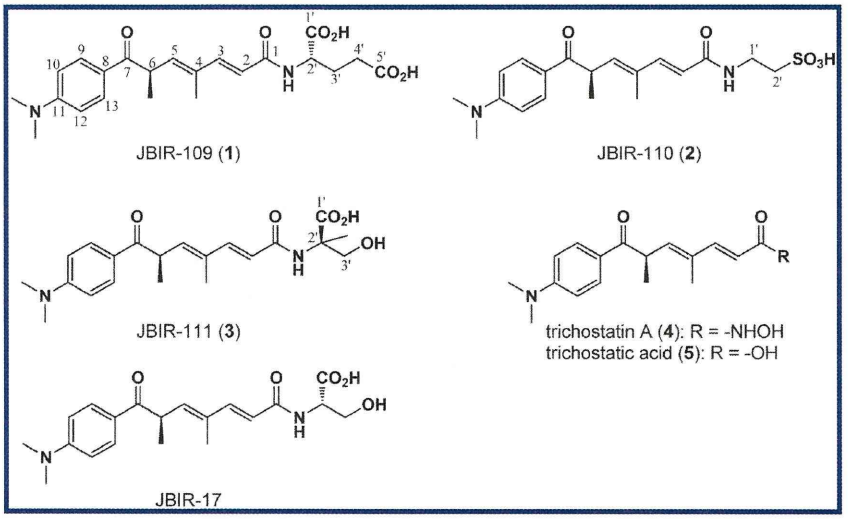

Table 1. ^{1}H (600 MHz) and ^{13}C (150 MHz) NMR Spectroscopic Data for JBIR-109 (1) in CD_3OD

position	δ_C, type	δ_H (J in Hz)
1	169.0, C	
2	120.3, CH	6.09, d (15.5)
3	146.6, CH	7.16, d (15.5)
4	134.5, C	
5	141.5, CH	5.91, d (9.5)
6	41.8, CH	4.53, dq (6.5, 9.5)
7	201.5, C	
8	124.8, C	
9, 13	132.0, CH	7.86, d (9.0)
10, 12	112.0, CH	6.73, d (9.0)
11	155.5, C	
4-methyl	12.8, CH_3	1.95, s
6-methyl	18.3, CH_3	1.27, d (6.5)
11-*N*,*N*-dimethyl	40.1, CH_3	3.06, s
Glu		
1′	175.3, C	
2′	53.5, CH	4.50, dd (6.0, 9.0)
3′	28.3, CH_2	2.20, m
		1.98, m
4′	31.4, CH_2	2.40, m
5′	176.5, C	

(δ_H 2.99), together with an HMBC correlation from H-1′ to amide carbonyl carbon C-1 (δ_C 168.7), revealed that an additional two-carbon fragment was present at the carboxy terminus of the trichostatic acid skeleton. The NMR spectra of the amino acid moiety [C-1′ (δ_H 3.67, δ_C 36.7) and C-2′ (δ_H 2.99, δ_C 51.4)] in **2** were similar to those of taurine [C-1′ (δ_H 3.55, δ_C 36.8) and C-2′ (δ_H 2.95, δ_C 51.5)] in the literature.[6] Finally, a sulfonic acid residue, the presence of which was deduced from the molecular formula, was attached to H-2′, establishing that **2** was a trichostatic acid analogue modified with taurine as shown in Figure 1.

The NMR spectroscopic data for **3** closely resembled those of JBIR-17. An HMBC correlation from the singlet methyl protons 3′-Me (δ_H 1.48) to carboxy carbonyl carbon C-1′ (δ_C 177.1), quaternary carbon C-2′ (δ_C 62.4), and a hydroxymethyl carbon (δ_C 66.0) suggested the presence of an α-methylserine moiety. The molecular formula of **3** indicated a C-2′-methylated congener of JBIR-17. In addition, the connectivity of trichostatic acid and the α-methylserine moiety was confirmed by NMR experiments in DMSO-d_6. HMBC correlations between the amide proton (δ_H 7.85) and C-1 (δ_C 164.6), C-1′ (δ_C 174.8), C-2′ (δ_C 60.0), C-3′ (δ_C 65.2), and 1′-methyl (δ_C 20.1) indicated that the α-methylserine connects to C-1 of trichostatic acid through an amide bond.

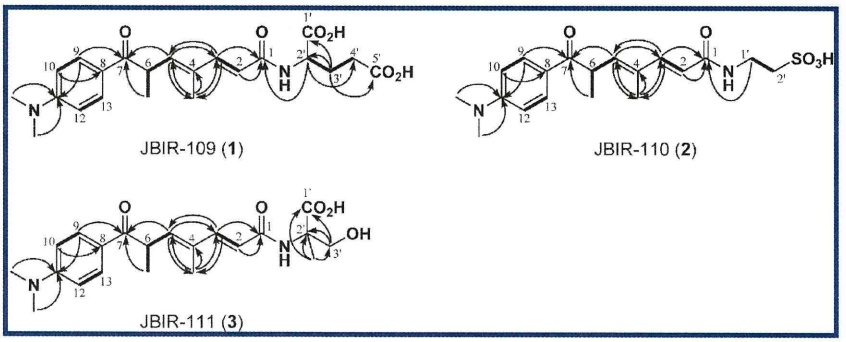

Figure 1. Key correlations observed in 2D NMR spectra of **1**, **2**, and **3**. Bold lines show ^{1}H–^{1}H DQF-COSY correlations, and arrows show HMBC results.

dx.doi.org/10.1021/np200843k | *J. Nat. Prod.* 2012, 75, 285–289

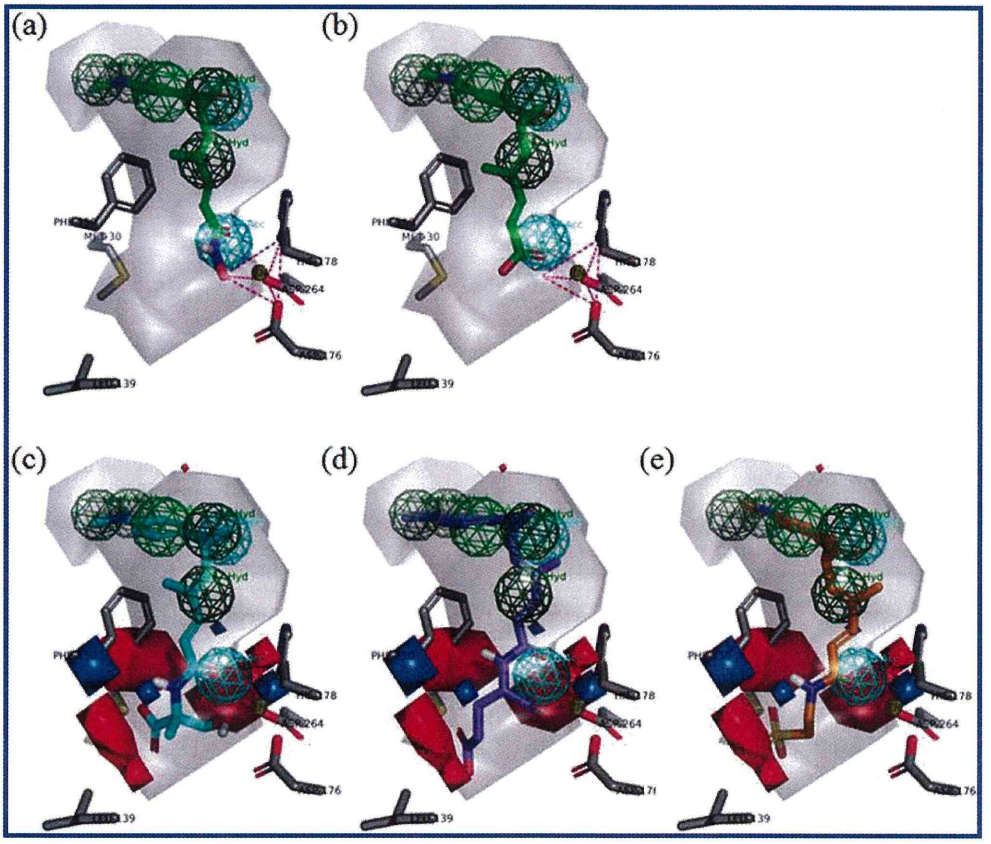

Figure 2. Proposed binding models for **4** (a), **5** (b), **1** (c), **2** (d), and **3** (e) to human HDAC1. Carbon atoms of **1** (purple, blue), **2** (orange), and **3** (cyan) are shown. Consensus features of the pharmacophore models are generated for the five molecules: hydrogen bond acceptor (cyan feature), aromatic ring region (green feature), and hydrophobic region (dark green feature). The shape of the overall volume for the five molecules is defined by the transparent surface. HDAC1 residues around the compounds are shown in stick (gray) representation. Tetrahedral zinc complexes in the protein cavity, which are composed of a nitrogen atom of a histidine residue, two carbonyl groups of aspartic acid residues, and the carbonyl group of the compounds, are represented by the polyhedral cage with purple dashed lines in (a) and (b). Red and blue in (c, d, e) show negative and positive regions, respectively, predicted by electrostatic analysis using 3D-QSAR.

The absolute configurations of the glutamic acid residue in **1** and the α-methylserine residue in **3** were defined by Marfey's method.[7] Comparisons of retention times between the FDAA-treated residues from the hydrolysates of standards established the configurations of the glutamic acid residue in **1** as L and the α-methylserine residue in **3** as *R*. It is intriguing to note that the configuration of the serine in **3** is opposite that of the serine in JBIR-17 isolated from another *Streptomyces* sp.[3] Because the specific rotation value ($[\alpha]^{25}_{D}$ +29, *c* 0.10, MeOH) of **4** isolated with **1**–**3** is of the same sign and similar to the value ($[\alpha]^{25}_{D}$ +63 (*c* 0.10, MeOH)[4]) reported for **4**, the absolute configurations of the trichostatic acid residues of **1**–**3** are proposed to be the same as for (*R*)-trichostatin A.[4]

To evaluate the HDAC inhibitory activity of **1**–**5**, we employed HDAC1 as a representative HDAC. The IC_{50} values against HDAC1 of **1**–**5** were 48, 74, 57, 0.012, and 73 μM, respectively. The inhibitory activities of **1**–**3** and **5** against HDAC1 were >1000 times weaker than that of **4**. These results are consistent with the reported model for HDAC1 inhibition by trichostatin A, in which the hydroxamate functionality is essential to exert the activity.[8] In addition, we performed computational binding analyses using the 3D-quantitative structure–activity relationship (QSAR) for **1**–**5** (Figure 2). The results show that the main reason for the low binding affinity of **5** to HDAC1 can be ascribed to the inability to form a stable tetrahedral zinc complex in the protein cavity. Meanwhile, the electrostatic analysis by 3D-QSAR showed that the low-binding affinity of **1**–**3** is due to an unfavorable interaction between the hydrophobic surface consisting of Leu-139, Phe-150, and Met-30 within the protein cavity and the polar functional groups in these compounds.

HDAC inhibitors are promising antitumor agents and also play important roles as low-molecular probes to study epigenetics. These results provide valuable information for developing new HDAC inhibitors.

EXPERIMENTAL SECTION

General Experimental Procedures. Optical rotations were measured using a Horiba SEPA-300 polarimeter. UV and IR spectra were measured with a Beckman Coulter DU730 UV/vis spectrophotometer and a Horiba FT-720 spectrophotometer, respectively. NMR spectra were collected in CD_3OD using a Varian NMR System 600 NB CL spectrometer with the residual solvent peaks referenced to δ_C 49.15 and δ_H 3.31 ppm. The optimizations of HMBC and HSQC spectra for appropriate couplings were 8 and 140 Hz, respectively. HRESIMS data were recorded using a Waters LCT-Premier XE mass spectrometer. Reversed-phase MPLC was conducted on a Purif-Pack ODS-100 column (Shoko Scientific). Analytical reversed-phase HPLC was conducted using an XBridge C18 column (4.6 i.d. × 150 mm;

dx.doi.org/10.1021/np200843k | *J. Nat. Prod.* 2012, 75, 285–289

Waters) in conjunction with a Waters 2996 photodiode array detector and a Waters 3100 mass detector. Analytical reversed-phase UPLC (Waters) was performed using a BEH ODS column (2.1 i.d. × 50 mm; Waters) in conjunction with a Waters ACQUITY UPLC photodiode array eλ detector and an LCT-Premier XE mass spectrometer. Preparative reversed-phase HPLC was conducted using an XBridge Prep C18 column (20 i.d. × 150 mm) in conjunction with a Hitachi High Technologies L-2455 photodiode array detector.

Biological Material. *Streptomyces* strain RM72 was isolated from an unidentified marine sponge collected at a depth of 195 m at the position 28° 53′ 35.8″ N, 129° 29′ 57.0″ E near Takara Island, Kagoshima Prefecture, Japan. To identify the strain, a partial 16S rRNA gene sequence was determined (DDBJ accession number AB683042), and comparison with sequences in the Eztaxon type strain database[9] revealed that the closest phylogenetic neighbor of the strain was *Streptomyces angustmycinicus* NBRC 3934^T (AB184817), with a sequence identity of 100%.

Fermentation. The strain was cultivated in 50 mL test tubes each containing 15 mL of the seed medium consisting of 1.0% starch (Kosokagaku), 1.0% Polypepton (Nihon Pharmaceutical), 1.0% molasses (Dai-Nippon Meiji Sugar), and 1.0% meat extract (Extract Ehlrich, Wako Pure Chemical Industry) (pH 7.2). The test tubes were shaken on a reciprocal shaker (320 rpm) at 27 °C for 2 days. Aliquots (2.5 mL) of the broth were then transferred to 500 mL baffled Erlenmeyer flasks containing 100 mL of the production medium consisting of 1.0% starch, 1.0% glucose (Kanto Chemical), 1.0% glycerin (Nacalai Tesque), 0.5% Polypepton, 0.2% yeast extract (BD Biosciences), 1.0% corn-steep liquor (Oriental Yeast), 0.1% NaCl (Kanto Chemical), and 0.32% $CaCO_3$ (Kozaki Pharmaceutical) in 50% artificial seawater (Marine art SF-1, Tomita Pharmaceutical) (pH 7.4 before sterilization) and cultured on a rotary shaker (180 rpm) at 27 °C for 5 days.

Isolation. The fermentation broth (2 L) was separated into the mycelial cake and supernatant by centrifugation. The supernatant was subsequently applied to a Diaion HP-20 column, and the column was then washed with H_2O and eluted with 100% MeOH. After evaporation of the 100% MeOH eluent *in vacuo*, the resulting residue was subjected to reversed-phase MPLC by using an aqueous MeOH linear gradient system (20–100% MeOH). The 20–30% MeOH eluate (145 mg) was then subjected to preparative reversed-phase HPLC with 55% aqueous MeOH containing 0.1% formic acid (flow rate, 6 mL/min) to give JBIR-109 (**1**, t_R = 13.7 min, 3.5 mg) and JBIR-110 (**2**, t_R = 11.3 min, 3.4 mg). In addition, the 30–40% MeOH eluate (107 mg) was purified by preparative reversed-phase HPLC using 58% aqueous MeOH containing 0.1% formic acid (flow rate, 6 mL/min) to give JBIR-111 (**3**, t_R = 13.7 min, 3.5 mg), trichostatin A (**4**, t_R = 11.3 min, 0.7 mg), and trichostatic acid (**5**, t_R = 13.0 min, 1.0 mg).

JBIR-109 (1): colorless, amorphous solid; $[\alpha]^{25}_D$ −27 (*c* 0.10, MeOH); UV (MeOH) λ_{max} (log ε) 340 (4.2), 265 (4.2) nm; IR (KBr) ν_{max} 1660 cm^{-1}; ^{1}H NMR (600 MHz, CD_3OD) and ^{13}C NMR (150 MHz, CD_3OD), see Table 1; HRESIMS *m/z* 417.2029 [M + H]$^+$ (calcd for $C_{22}H_{29}N_2O_6$, 417.2026).

JBIR-110 (2): colorless, amorphous solid; $[\alpha]^{25}_D$ +12 (*c* 0.10, MeOH); UV (MeOH) λ_{max} (log ε) 340 (4.2), 264 (4.2) nm; IR (KBr) ν_{max} 1660 cm^{-1}; ^{1}H NMR (600 MHz, CD_3OD) and ^{13}C NMR (150 MHz, CD_3OD), see Table 2; HRESIMS *m/z* 395.1655 [M + H]$^+$ (calcd for $C_{19}H_{27}N_2O_5S$, 395.1641).

JBIR-111 (3): colorless, amorphous solid; $[\alpha]^{25}_D$ +33 (*c* 0.10, MeOH); UV (MeOH) λ_{max} (log ε) 340 (4.1), 265 (4.2) nm; IR (KBr) ν_{max} 1650 cm^{-1}; ^{1}H NMR (600 MHz, CD_3OD) and ^{13}C NMR (150 MHz, CD_3OD), see Table 2; HRESIMS *m/z* 389.2067 [M + H]$^+$ (calcd for $C_{21}H_{29}N_2O_5$, 389.2076).

Determination of Amino Acid Configurations. A sample of **1** or **3** (1.0 mg) was hydrolyzed in 6 N HCl (0.2 mL) at 110 °C for 12 h. After acid hydrolysis, the reaction solution was adjusted to neutral pH and evaporated *in vacuo*. The residue was dissolved in 10 mL of EtOAc–H_2O (1:1). The amino acid mixture was then recovered in the aqueous layer. After drying the aqueous layer *in vacuo*, it was dissolved in 5% $NaHCO_3$ (600 μL), and FDAA (Marfey's reagent, 0.2 mg) in acetone (600 μL) was added. The mixture was then heated in an oil bath at 70 °C for 10 min with frequent shaking. The reaction products were analyzed by the UPLC system. A Waters BEH ODS column was developed with 20% aqueous MeCN containing 0.1% formic acid at a flow rate of 0.3 mL/min. The retention times of the FDAA derivatives were determined by monitoring UV absorption at 340 nm and the positive mode of ESIMS. The retention times of the standard FDAA derivatives were as follows: L-Glu, 2.34 min; D-Glu, 2.95 min; α-methyl-*R*-Ser, 2.10 min; and α-methyl-*S*-Ser, 2.74 min. The retention times of the FDAA derivatives from **1** and **3** were 2.38 min for Glu and 2.10 for α-methyl-Ser, respectively.

Table 2. ^{1}H (600 MHz) and ^{13}C (150 MHz) NMR Spectroscopic Data for Amino Acid Moieties of JBIR-110 (2) and JBIR-111 (3) in CD_3OD

JBIR-110 (2)			JBIR-111 (3)		
position	δ_C, type	δ_H (*J* in Hz)	position	δ_C, type	δ_H (*J* in Hz)
Taurine			MeSer		
1′	36.7, CH_2	3.67, t (6.6)	1′	177.1, C	
2′	51.4, CH_2	2.99, t (6.6)	2′	62.4, C	
			3′	66.0, CH_2	3.90, brd (11.0)
					3.85, brd (11.0)
			3′-methyl	20.8, CH_3	1.48, s

HDAC1 Inhibitory Assay. The human HDAC1 inhibitory activity was evaluated using the HDAC1 inhibitor screening assay kit (Cayman Chemical) according to the manufacturer's protocol. Briefly, 140 μL of assay buffer, 10 μL of diluted HDAC1, and 10 μL of samples were added in a 96-well black plate. To initiate the reaction, 10 μL of the HDAC substrate (final concentration, 200 μM) was added. After incubation for 30 min at 37 °C, 40 μL of the developer was added and mixed. After further incubation for 15 min at room temperature, the fluorescence (excitation, 340 nm; emission, 450 nm) was measured. Trichostatin A was used as a positive control (IC_{50} = 12 nM).

Quantitative Structure–Activity Relationship. 3D-QSAR analysis for compounds **1**–**5** was carried out using the homology model of HDAC1 and the docking simulation. A three-dimensional structure of human HDAC1 was constructed by a homology modeling approach with the structural template of the crystal structure of an HDAC homologue complexed with trichostatin A (PDB-ID: 1C3R),[10] incorporated in the program Prime with default parameters (Schrödinger, LLC). The sequence identity between HDAC1 and the HDAC homologue protein was 32% (see Supporting Information, Figure 24S). The structural template was selected by using a similarity measure from the sequence-structure alignment and in addition from the protein–ligand interactions in the active-site environment obtained by induced fit modeling. To prepare the compounds with active conformations for 3D-QSAR analysis, molecular models of the compound-bound HDAC1 were generated by docking simulation using Glide SP mode with default parameters (Schrödinger, LLC). The grid center for docking was defined using the reference position of trichostatin A on 1C3R, which is the structural template used in the homology modeling step. 3D-QSAR analysis with the aligned active conformation from docking results was performed using the Auto-GPA protocol on MOE (Chemical Computing Group). The visualizations were generated by PyMOL (Schrödinger, LLC).

■ ASSOCIATED CONTENT

Supporting Information

^{1}H and ^{13}C NMR, DQF-COSY, HSQC, CT-HMBC, and HRESIMS spectra of **1**–**3** are available free of charge via the Internet at http://pubs.acs.org.

dx.doi.org/10.1021/np200843k | *J. Nat. Prod.* 2012, 75, 285–289

AUTHOR INFORMATION

Corresponding Author

*(M.T.) Tel: +81-3-3599-8305. Fax: +81-3-3599-8494. E-mail: motoki-takagi@aist.go.jp. (K.S.) Tel: +81-3-3599-8305. Fax: +81-3-3599-8494. E-mail: k-shinya@aist.go.jp.

ACKNOWLEDGMENTS

This work was supported by a grant from the New Energy and Industrial Technology Department Organization (NEDO). The sponge was collected during the NT-09-17 cruise of Natsushima, by the Japan Agency for Marine-Earth Science and Technology (JAMSTEC).

REFERENCES

(1) Carew, J. S.; Giles, F. J.; Nawrocki, S. T. *Cancer Lett.* **2008**, *269*, 7−17.

(2) Shankar, S.; Srivastava, R. K. *Adv. Exp. Med. Biol.* **2008**, *615*, 261−298.

(3) Ueda, J.; Hwang, J. H.; Maeda, S.; Kato, T.; Ochiai, A.; Isshiki, K.; Yoshida, M.; Takagi, M.; Shin-ya, K. *J. Antibiot.* **2009**, *62*, 283−285.

(4) Morikawa, H.; Ishihara, M.; Takezawa, M.; Hirayama, K.; Suzuki, E.; Komoda, Y.; Shibai, H. *Agric. Biol. Chem.* **1985**, *49*, 1365−1370.

(5) Tsuji, N.; Kobayashi, M.; Nagashima, K.; Wakisaka, Y.; Koizumi, K. *J. Antibiot.* **1976**, *29*, 1−6.

(6) Bi, D.; Chai, X.-Y.; Song, Y.-L.; Lei, Y.; Tu, P.-F. *Chem. Pharm. Bull.* **2009**, *57*, 528−531.

(7) Marfey, P. *Carlsberg Res. Commun.* **1984**, *49*, 591−596.

(8) Yoshida, M.; Kijima, M.; Akita, M.; Beppu, T. *J. Biol. Chem.* **1990**, *265*, 17174−17179.

(9) Chun, J.; Lee, J. H.; Jung, Y.; Kim, M.; Kim, S.; Kim, B. K.; Lim, Y. W. *Int. J. Syst. Evol. Microbiol.* **2007**, *57*, 2259−2261.

(10) Finnin, M. S.; Donigian, J. R.; Cohen, A.; Richon, V. M.; Rifkind, R. A.; Marks, P. A.; Breslow, R.; Pavletich, N. P. *Nature* **1999**, *401*, 188−193.

View Online / Journal Homepage / Table of Contents for this issue

Dynamic Article Links

Organic & Biomolecular Chemistry

Cite this: *Org. Biomol. Chem.*, 2012, **10**, 736

www.rsc.org/obc

PAPER

Cyclopropane-based stereochemical diversity-oriented conformational restriction strategy: Histamine H_3 and/or H_4 receptor ligands with the 2,3-methanobutane backbone

Mizuki Watanabe,[a] Takaaki Kobayashi,[a] Takatsugu Hirokawa,[b] Akira Yoshida,[c] Yoshihiko Ito,[c] Shizuo Yamada,[c] Naoki Orimoto,[d] Yasundo Yamasaki,[d] Mitsuhiro Arisawa[a] and Satoshi Shuto*[a]

Received 1st September 2011, Accepted 11th October 2011
DOI: 10.1039/c1ob06496g

The stereochemical diversity-oriented conformational restriction strategy can be an efficient method for developing specific ligands for drug target proteins. To develop potent histamine H_3 and/or H_4 receptor ligands, a series of conformationally restricted analogs of histamine with a chiral *trans*- or *cis*-4-amino-2,3-methano-1-(1*H*-imidazol-4-yl)butane structure was designed based on this strategy. These stereochemically diverse compounds were synthesized from previously developed versatile chiral cyclopropane units. Among these analogs, a *trans*-cyclopropane-type compound, (2*S*,3*R*)-4-(4-chlorobenzylamino)-2,3-methano-1-(1*H*-imidazol-4-yl)butane (**5b**), has remarkable antagonistic activity to both the H_3 (K_i = 4.4 nM) and H_4 (K_i = 5.5 nM) receptors, and a *cis*-cyclopropane-type compound, (2*R*,3*R*)-4-amino-2,3-methano-1-(1*H*-imidazol-4-yl)butane (**6a**), is a potent and selective H_3 receptor partial agonist (K_i = 5.4 nM). Although (2*S*,3*R*)-4-amino-2,3-methano-1-(1*H*-imidazol-4-yl)butane (**5a**) does not have a hydrophobic group which the usual H_3 receptor antagonists have, it was found to be a potent H_3 receptor antagonist (K_i = 20.1 nM). Thus, a variety of compounds with different pharmacological properties depending on the cyclopropane backbones and also on the side-chain functional groups were identified. In addition to the previously used 1,2-methanobutane backbone, the 2,3-methanobutane backbone also worked effectively as a cyclopropane-based conformational restriction structure. Therefore, the combination of these two cyclopropane backbones increases the stereochemical and three-dimensional diversity of compounds in this strategy, which can provide a variety of useful compounds with different pharmacological properties.

Introduction

The histamine H_3 receptor, a member of the G_i protein-coupled receptors (GPCRs) distributed mainly in the central nervous system, is of interest as a potential drug target.[1] Agonists and antagonists to the H_3 receptor are considered to be potential drugs for the treatment of sleep disorders, migraines, asthma, inflammation, or ulcers,[2a] and for the treatment of Alzheimer's disease, attention-deficit/hyperactivity disorder (ADHD), schizophrenia, depression, dementia, or epilepsy,[2b] respectively.

On the other hand, the histamine H_4 receptor, also one of the GPCRs, is expressed in immunocytes, such as eosinophils or mast cells, and chemotaxis of these cells *via* histamine is triggered through H_4 receptor activation.[3a] Accordingly, H_4 receptor antagonists may be effectively used in new therapeutic modalities for the treatment of allergic diseases.[3b,c]

Although GPCRs, including the H_3 and H_4 receptors, are important targets for drug development,[4] structural analysis of GPCRs is difficult due to the membranous nature of these proteins and to their very low natural abundance, compared with that of proteins soluble in blood or cytosol.[5] Therefore, structural data on the drug target GPCRs are generally poor, and a method for effectively identifying compounds that target GPCRs without any structural data is required in drug development. Thus, we previously reported a stereochemical diversity-oriented conformational restriction strategy to develop compounds that bind selectively to structure-unknown target proteins such as GPCRs.[6,7] To realize the strategy, we devised versatile chiral cyclopropane units with different stereochemistries,[6a,c] shown in Fig. 1, and, by using these units, a series of cyclopropane-based conformationally restricted analogs[8] with

[a]*Faculty of Pharmaceutical Sciences, Hokkaido University, Kita-ku, Sapporo, 060-0812, Japan. E-mail: shu@pharm.hokudai.ac.jp*
[b]*Computational Biology Research Center, National Institute of Advanced Industrial Science and Technology, Aomi, Koutou-ku, Tokyo, 135-0064, Japan*
[c]*Department of Pharmacokinetics and Pharmacodynamics and Global Center of Excellence (COE), School of Pharmaceutical Sciences, University of Shizuoka, 52-1 Yada, Suruga-ku, Shizuoka, 422-8526, Japan*
[d]*Hanno Research Center, Taiho Pharmaceutical Co. Lrd., Misugidai, Hanno, 357-8527, Japan*

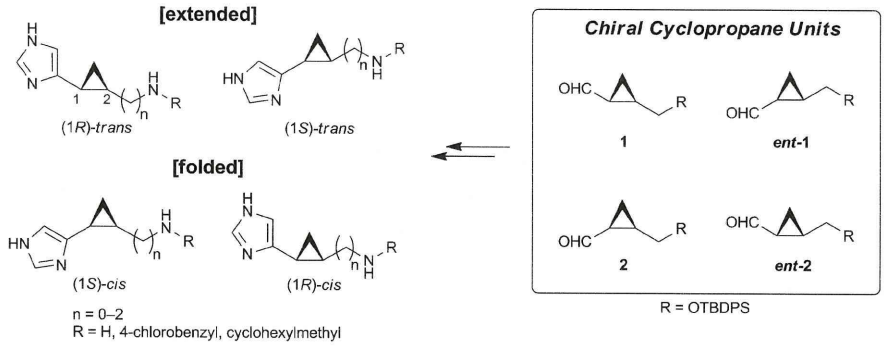

Fig. 1 Conformationally restricted analogs of histamine having the 1,2-methanoalkylimidazole backbone prepared from chiral cyclopropane units.

stereochemical diversity can be designed and synthesized effectively.

Based on the strategy, we actually designed a series of conformationally restricted analogs of histamine with different stereochemistries, which were synthesized from the chiral cyclopropane units (Fig. 1).[6] In these conformationally restricted analogs having an aminoalkyl-1,2-methanoimidazole backbone, the imidazole and the amino side-chain moieties are located in a variety of spatial arrangements due to the conformationally restricted 1,2-methanoalkyl backbone. Consequently, a series of these analogs is not only stereochemically diverse but also three-dimensionally diverse as a molecule. Some of these analogs shown in Fig. 2 were identified as potent histamine receptor ligands; *e.g.*, AEIC (**3**) with a (1*S*)-*cis*-cyclopropane structure is the first highly selective H_3 receptor agonist,[6b] and (1*R*,2*S*)-2-[2-(4-chlorobenzylamino)ethyl]-1-(1*H*-imidazol-4-yl)cyclopropane [(*R*)-CEIC (**4**)] with a (1*R*)-*trans*-cyclopropane structure and its enantiomer (*S*)-CEIC (***ent*-4**) with a (1*S*)-*trans*-cyclopropane structure were highly potent antagonists to both the H_3 receptor and the H_4 receptor.[6c]

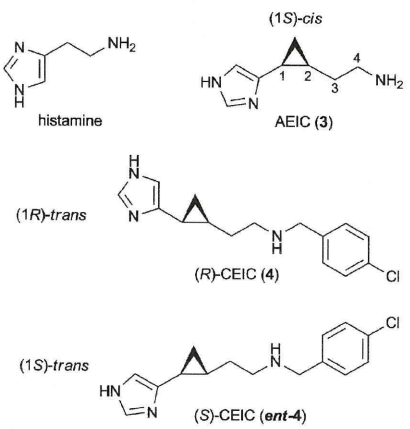

Fig. 2 Histamine and its conformationally restricted analogs having the 1,2-methanobutylimidazole backbone.

In the course of our studies to develop further potent H_3 and H_4 receptor ligands, we newly designed a series of conformationally restricted analogs of histamine based on the stereochemical diversity-oriented strategy, namely **5a,b** and **6a,b**, and their enantiomers, ***ent*-5a,b** and ***ent*-6a,b**, all having a 2,3-methanobutylimidazole structure (Fig. 3). In this report, we

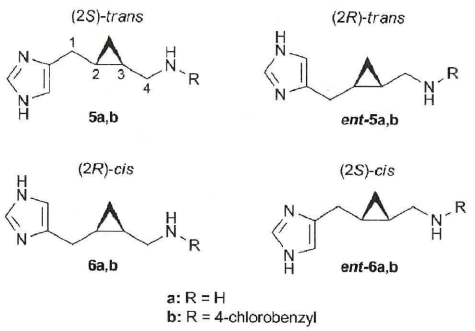

Fig. 3 Conformationally restricted analogs of histamine having the 2,3-methanobutylimidazole backbone.

describe the design, synthesis, and pharmacological effects of these compounds.

Results and discussion

Design of compounds

Our previous studies demonstrated that conformational restriction of histamine by the 4-amino-1,2-methanobutane backbone was effective for the H_3 and/or H_4 receptor binding, where the folded *cis*-cyclopropane structure like AEIC (**3**) and the extended *trans*-cyclopropane structure like (*R*)- and (*S*)-CEIC (**4** and ***ent*-4**) are suitable for the binding as an agonist and an antagonist, respectively.[6b,c] They also showed that functional conversion of an agonist into an antagonist could occur by introducing a hydrophobic group, such as a chlorobenzyl group,[2b] at the terminal primary amino moiety of the 4-amino-1,2-methanobutane backbone.[6c] Considering these results, we designed the regioisomeric derivatives of AEIC (**3**) and (*R*)- and (*S*)-CEIC (**4** and ***ent*-4**), which have a 4-amino-2,3-methanobutane backbone, as shown in Fig. 3, for identifying new H_3 and/or H_4 receptor ligands. In these compounds, the folded *cis*-cyclopropane or the extended *trans*-cyclopropane structure on the four carbon (butane) backbone is preserved, and accordingly, the imidazole and the basic nitrogen moieties, which are key components in these structures for binding to the histamine receptors, might be located in space similarly to those of the previously identified potent analogs having the 4-amino-1,2-methanobutane backbone. Also, the regioisomeric 2,3-methano structure could change spatial arrangement and flexibility around the imidazole and the basic

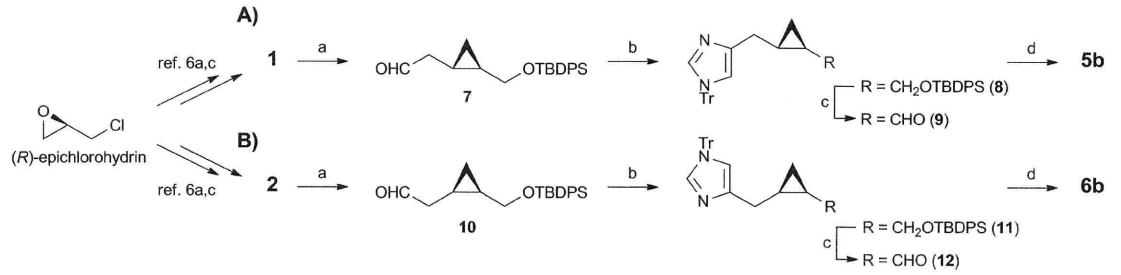

Scheme 1 *Conditions*: a) 1) $MeOCH_2PPh_3Cl$, $NaN(TMS)_2$, THF, 0 °C, 2) HCl, aq. acetone, 0 °C, 85% (**7**), 92% (**10**); b) 1) $TosCH_2NC$, NaCN, EtOH, 0 °C, 2) sat. NH_3 in EtOH, steel tube, 120 °C, 3) TrCl, pyridine, 48% (**8**), 51% (**11**); c) 1) TBAF, THF, 2) Dess–Martin periodinane, CH_2Cl_2, 78% (**9**), 65% (**12**); d) 1) 4-chlorobenzylamine, 2-picoline borane, AcOH, MeOH, 2) TrCl, Et_3N, CH_2Cl_2, 3) HCl, aq. EtOH, 78 °C, 30% (**5b**), 49% (**6b**).

nitrogen moieties, compared with those in the 1,2-methano lead compounds AEIC (**3**) and (*R*)- and (*S*)-CEIC (**4** and ***ent*-4**), which would affect the biological activity. We hoped to develop both agonists and antagonists, and therefore, compounds with a free primary amino function (**a**-series, as agonists) and compounds with a 4-chlorobenzylamino function (**b**-series, as antagonists) were designed for synthesis.

Thus, we expected that the 2,3-methanobutane backbone might be useful as an alternative conformationally restricted structure in the cyclopropane-based stereochemical diversity-oriented strategy.

Chemistry

Although much effort has been devoted to developing practical methods for preparing chiral cyclopropanes, synthesizing cyclopropane derivatives with a desired stereochemistry is often troublesome.[9] We devised the chiral units (Fig. 1), which are composed of four stereoisomeric cyclopropane derivatives bearing two adjacent carbon substituents in a *trans* or *cis* relationship, namely **1** and **2**, and their enantiomers, ***ent*-1** and ***ent*-2**, for cyclopropane-based conformational restriction.[6a] These units, which are generally useful for synthesizing various compounds having an asymmetric *trans*- or *cis*-cyclopropane structure,[6] were employed as the key intermediates in this study.

The synthesis of the *trans*-cyclopropane compound **5b** and the *cis*-cyclopropane compound **6b** with a 4-chlorobenzyl group (**b**-series) from the chiral cyclopropane unit **1** and **2**, respectively, is shown in Scheme 1. These units **1** and **2** were prepared from (*R*)-epichlorohydrin according to the method reported previously.[6a,c] The Wittig reaction of the unit **1** with $MeOCH_2PPh_3Cl/NaN(TMS)_2$, followed by acidic treatment gave the one carbon-elongated aldehyde **7**. The imidazole ring was constructed by treating **7** with tosylmethyl isocyanide and NaCN followed by heating in NH_3/EtOH.[10] The resulting imidazole product without purification was further treated with TrCl in pyridine to give the *N*-tritylimidazolylmethylcyclopropane derivative **8** in 48% overall yield. After removal of the silyl-protecting group of **8**, the resulting cyclopropanemethanol was oxidized to afford the aldehyde **9**. Introduction of a 4-chlorobenzylamino function at the terminal carbon was next investigated under reductive amination conditions. Thus, treatment of the aldehyde **9** with 4-chlorobenzylamine and 2-picoline borane in AcOH/MeOH, and subsequent acidic removal of the trityl group of the product gave the desired *trans*-cyclopropane-type target compound **5b** (Scheme 1A). By a similar procedure, the *cis*-cyclopropane-type target compound **6b** was synthesized from the *cis*-cyclopropane unit **2** (Scheme 1B). The enantiomers, ***ent*-5b** and ***ent*-6b**, were also synthesized from ***ent*-1** and ***ent*-2**, respectively.

The synthesis of **5a** and **6a** with a terminal primary amine (**a**-series) is shown in Scheme 2. Treatment of the aldehyde **9** with *t*-BuS(O)NH_2 and $CuSO_4$ in CH_2Cl_2 gave the corresponding sulfinylimine product, which was, without purification, reduced with $NaBH_4$/MeOH to afford the sulfinylamide **13**. Simultaneous removal of the trityl and sulfinyl groups by treating **13** with HCl in EtOH produced the target *trans*-cyclopropane-type compound **5a** (Scheme 2A). Similarly, the *cis*-cyclopropane-type compound **6a** was prepared from the *cis*-cyclopropane aldehyde **12** (Scheme 2B). The corresponding enantiomers, ***ent*-5a** and ***ent*-6a**, were also synthesized from the *trans*- and *cis*-cyclopropane aldehydes, ***ent*-9** and ***ent*-12**, respectively.

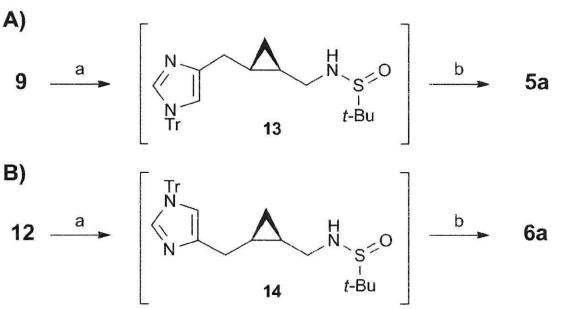

Scheme 2 *Conditions*: a) 1) *t*-BuS(O)NH_2, $CuSO_4$, CH_2Cl_2, 2) $NaBH_4$, MeOH, 0 °C; b) HCl, EtOH, 78 °C, 50% from **9** (**5a**), 59% from **12** (**6a**).

Pharmacological effects

The binding affinities of the conformationally restricted analogs with the 2,3-methanobutane backbone for the human H_3 receptor subtype using [^{3}H]N^α-methylhistamine and also for the human H_4 receptor subtype using [^{3}H]histamine were investigated, according to the previously reported procedure.[6c]

The binding affinities of the compounds for the H_3 receptor are summarized in Table 1. All of the synthesized compounds inhibited the specific binding of [^{3}H]N^α-methylhistamine to the H_3 receptor in a concentration-dependent manner. Of these compounds, all the *trans*-analogs, **5a**, ***ent*-5a**, **5b**, and ***ent*-5b**, had

Table 1 Effects of compounds on the human H_3 and H_4 receptor subtypes[a]

Compound	Structure	H_3			H_4			Selectivity
		K_i (nM)	act.[b] (%)	inh.[c] (%)	K_i (nM)	act.[b] (%)	inh.[c] (%)	$K_i(H_3)/K_i(H_4)$
5a	2,3-M[d]/(2*S*)-*trans*	20.1 ± 5.1	2.5	94	119 ± 25	11	45	0.17
***ent*-5a**	2,3-M/(2*R*)-*trans*	9.3 ± 0.8	17	72	50.9 ± 11	30	40	0.18
6a	2,3-M/(2*R*)-*cis*	5.4 ± 1.1	18	57	113 ± 30	24	–1.4	0.048
***ent*-6a**	2,3-M/(2*S*)-*cis*	172 ± 39	5.0	41	222 ± 23	47	6.4	0.77
5b	2,3-M/(2*S*)-*trans*	4.4 ± 0.2	0	99	5.5 ± 0.6	0	100	0.80
***ent*-5b**	2,3-M/(2*R*)-*trans*	21.1 ± 5.1	0	99	23.2 ± 3.6	5.0	94	0.91
6b	2,3-M/(2*R*)-*cis*	110 ± 16	1.8	90	172 ± 40	3.2	72	0.64
***ent*-6b**	2,3-M/(2*S*)-*cis*	103 ± 13	6.7	86	33.5 ± 2.9	15	68	3.1
AEIC (**3**)[e]	1,2-M[d]/(1*S*)-*cis*	1.3 ± 0.2	100	—	—	—	—	—
(*R*)-CEIC (**4**)[f]	1,2-M/(1*R*)-*trans*	8.4 ± 1.5	0	100	7.6 ± 0.4	0	>100	1.1
(*S*)-CEIC (***ent*-4**)[f]	1,2-M/(1*S*)-*trans*	3.6 ±0.4	0	100	37.2 ±2.7	0	>100	0.097
Thioperamide[f]	—	51.1 ± 3.8	—	99	124 ±14	—	90	0.41

[a] Assay was carried out with cell membranes expressing human H_3 or H_4 receptor subtypes (n = 3–4). [b] Relative potency of compound (10^{-5} M) to histamine (10^{-5} M) for the receptor activation. [c] Inhibitory effect of compound (10^{-5} M) on the agonistic activity of histamine (10^{-6} M). [d] 1,2-M and 2,3-M mean 1,2-methano and 2,3-methano, respectively. [e] Data with rat H_3 receptor taken from ref. 6b. [f] Data taken from ref. 6c.

remarkably more potent activity (K_i < 30 nM) than the well-known H_3 receptor antagonist thioperamide (K_i = 51.1 nM). On the other hand, the *cis*-analogs showed relatively weaker affinity for the H_3 receptor than the *trans*-analogs, except for the (2*R*)-*cis*-analog **6a** (K_i = 5.4 nM). In order of the binding affinities, these compounds ranked as **5b**, **6a** > ***ent*-5a** > **5a**, ***ent*-5b** > ***ent*-6b**, **6b** > ***ent*-6a**, where ***ent*-5a**, **6a**, and **5b** had a significant nM level K_i.

The binding affinities of the compounds for the human H_4 receptor subtype are also summarized in Table 1. The *trans*-analogs, **5b**, ***ent*-5b**, and *cis*-analog ***ent*-6b** had significant activity ($K_i \leq$ 30 nM), with **5b** being the most potent (K_i = 5.5 nM).

The relative affinity of these compounds for the H_3 and the H_4 receptors would indicate that a hydrophobic group might be required for high affinity for the H_4 receptor but not for the H_3 receptor, as shown with the non-hydrophobic analog **6a** (K_i = 5.4 nM for H_3, K_i = 113 nM for H_4) and the hydrophobic analog **5b** (K_i = 4.4 nM for H_3, K_i = 5.5 nM for H_4). Our results are consistent with the previous reports on the histamine receptor ligands.[11]

The function of the compounds on human histamine H_3 and H_4 receptor subtypes, which were expressed individually in 293-EBNA cells, was next investigated by luciferase reporter gene assay.[6b] The results are also summarized in Table 1.

All the **b**-series compounds having a hydrophobic 4-chlorobenzyl function were antagonists in accordance with the previous results of the histamine receptor ligands.[2b,6c] The (2*S*)-*trans*-analog **5b** with the 2,3-methanobutane backbone was a highly potent antagonist to both the H_3 and H_4 receptors with K_i values of 4.4 nM (for H_3) and 5.5 nM (for H_4), which was more potent than its regioisomeric parent compound (*R*)-CEIC (**4**) with the 1,2-methanobutane backbone. While (*S*)-CEIC (***ent*-4**) with the 1,2-methanobutane backbone was a H_3 receptor selective antagonist (K_i (H_3)/K_i (H_4) = 0.097), its regioisomeric *trans*-analog ***ent*-5b** with the 2,3-methanobutane backbone showed non-selective moderate antagonistic effects on both of the receptors (K_i (H_3)/K_i (H_4) = 0.91).

Based on the previous SAR studies on H_3 and H_4 receptor ligands,[2a,6b] we expected that the **a**-series compounds having the primary amino side-chain without a hydrophobic group would be full agonists. However, the activation potencies for the receptors of these compounds relative to histamine were less than 50%, as shown in Table 1. These results indicate that ***ent*-5a**, **6a**, and ***ent*-6a** work as partial agonists to both of the H_3 and H_4 receptors. Furthermore, compound **5a** with the (2*S*)-*trans*-cyclopropane structure almost completely inhibited activation of the H_3 receptor by histamine (94% inhibition). Thus, although **5a** does not have a hydrophobic group which H_3 receptor antagonists usually have, unexpectedly, it was shown to be an H_3 receptor antagonist.[12] Compound **6a** is the regioisomeric *cis*-2,3-methanobutane analog of the parent compound AEIC (**3**) with the *cis*-1,2-methanobutane backbone, and both **6a** and **3** are selectively and highly active at the H_3 receptor (K_i = 5.4 nM and 1.3 nM, respectively). However, these two regioisomers have functionally different effects on the receptor, *i.e.*, **6a** was a partial agonist (18% activation), while **3** was a full agonist (100% activation).

Docking simulation by homology modeling

We previously constructed a three-dimensional model of the H_3 receptor[6d] based on a structural template from the crystal structure of the human β_2-adrenergic GPCR recently reported by Cherezov and co-workers.[5a] Using the model, docking simulations of a series of cyclopropane-based H_3 receptor ligands were performed and a reliable correlation between binding score and pK_i was obtained.[6d]

Therefore, in order to investigate the binding modes of the conformationally restricted analogs with the 2,3-methanobutane backbone to the H_3 receptor, docking simulations of the three potent ligands (***ent*-5a**, **6a**, and **5b**) and also the three less potent ligands (***ent*-6a**, **6b**, and ***ent*-6b**) were carried out by using the H_3 receptor homology model described above, and the binding modes were compared with that of AEIC (**3**) with the 1,2-methanobutane backbone. As shown in Fig. 4a, the proposed binding modes of the three potent ligands are well-superimposed with that of the potent lead compound **3**, especially at the imidazole ring and the basic nitrogen, which are important for the binding to the receptor. On the other hand, as shown in Fig. 4b, the proposed binding modes of the three less potent ligands and that of **3** are not as well superimposed. These results suggest that this homology

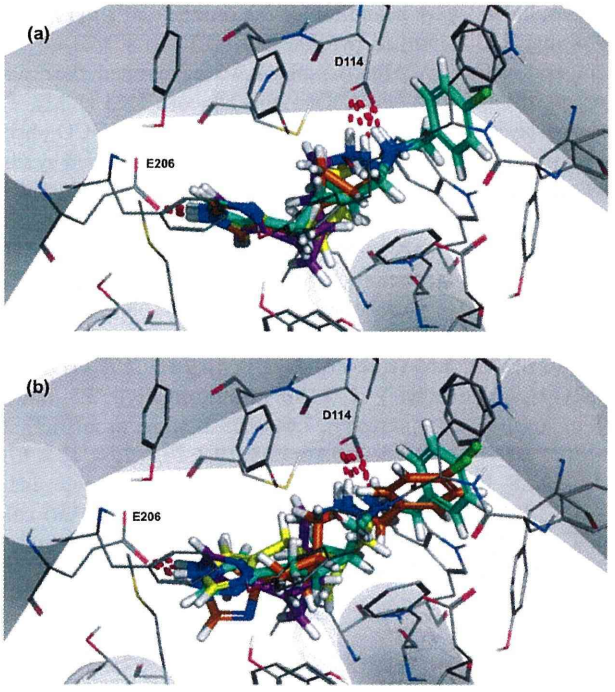

Fig. 4 Proposed models for the three potent ligands ***ent*-5a**, **6a**, **5b** and the lead compound **3** (a) and the three less potent ligands **6b**, ***ent*-6a**, ***ent*-6b** and **3** (b) binding to the homology model of the H_3 receptor[6d] from docking simulation. Carbon atoms are shown in magenta for **3**, cyan for **5b** and **6b**, yellow for **6a** and ***ent*-6a**, and orange for ***ent*-5a** and ***ent*-6b**, respectively. Hydrogen bonding and salt bridge between side-chain carboxyl group of Glu206 and an imidazole of the ligands, and between that of Asp114 and an amino group of the ligands are depicted by red dots.

model can be useful for investigation the binding modes of the H_3 receptor ligands and that the bioactive conformations of these potent ligands are analogous.

As described above, the stereochemical diversity-oriented conformational restriction strategy, employing the 2,3-methanobutane backbone, was shown to be useful for developing potent ligands of the H_3 and/or H_4 receptor in this study. It is important to note that, in addition to the previously used 1,2-methanobutane backbone, the regioisomeric 2,3-methanobutane backbone also worked effectively as an alternative cyclopropane-based conformational restriction structure. Thus, the combinational use of these two backbones not only increases the stereochemical diversity but also increases three-dimensional structural diversity of the compounds in this strategy, which can provide a variety of active compounds with different pharmacological properties.

Conclusions

We designed a series of conformationally restricted histamine analogs with a chiral *trans*- or *cis*-2,3-methanobutane backbone based on the stereochemical diversity-oriented strategy. These four stereochemical types of analogs were systematically synthesized from optically active epichlorohydrins *via* the versatile chiral cyclopropane units. Pharmacological properties of these analogs for the human H_3 and H_4 receptors were shown to be different depending on the stereochemistry of the cyclopropane backbones. Among the hydrophobic analogs (**b**-series), a *trans*-cyclopropane structure was preferred to a *cis*-cyclopropane one for both the H_3 and H_4 receptors. On the other hand, among the non-hydrophobic analogs (**a**-series), the structure of the most potent analog **6a** to both of the receptor subtypes was a *cis*-cyclopropane. In this study, a couple of potent H_3 and/or H_4 receptor ligands with a low nM K_i were identified. Analog **6a**, which has a (2*R*)-*cis*-2,3-methanobutane backbone, was the highest selective H_3 ligand, and analog **5b**, which has a (2*S*)-*trans*-2,3-methanobutane backbone, was the most potent H_3/H_4 dual ligand. Thus, the 2,3-methanobutane backbone worked effectively as the backbone of the conformationally restricted histamine analogs with stereochemical diversity as well as the 1,2-methanobutane. These differences in the stereochemistry of these backbones affected the potency and selectivity of the ligands. Therefore, the stereochemical diversity-oriented approach can be an effective strategy in medicinal chemistry studies.

Experimental

Chemical shifts (δ) are reported in ppm downfield from Me_4Si or CD_2HOD (3.31 ppm) (^1H) and $CDCl_3$ (77.0 ppm) or CD_3OD (49.0 ppm) (^{13}C). All of the ^1H-NMR assignments described were in agreement with COSY spectra. Thin-layer chromatography was done on Merck coated plate $60F_{254}$. Silica gel, Iatron beads and NH silica gel chromatographies were done on Merck silica gel 5715, Iatron 6RS-8060 (Mitsubishi Kagaku Iatron, Inc), and Chromatorex® (Fuji Silysia Chemical Ltd.), respectively. Reactions were carried out under an argon atmosphere except for hydrous reactions.

(2*S*,3*R*)-4-*tert*-Butyldiphenylsilyloxy-2,3-methanobutyraldehyde (7)

To a suspension of $MeOCH_2PPh_3Cl$ (3.63 g, 10.6 mmol) in THF (50 mL) was added $NaN(TMS)_2$ (1.0 M in THF, 9.12 mL, 9.12 mmol) at 0 °C, and the mixture was stirred at the same temperature for 20 min. To the resulting solution was added a solution of **1**[6a] (2.27 g, 7.60 mmol) in THF (10 mL) at 0 °C, and the reaction mixture was stirred at the same temperature for 5 h. After addition of saturated aqueous NH_4Cl, the solvent was evaporated, and the residue was partitioned between AcOEt and saturated aqueous NH_4Cl. The organic layer was washed with brine, dried (Na_2SO_4) and evaporated. The residue was purified by silica gel column chromatography (3% AcOEt in hexane) to give the enol ether product as an oil. To a solution of the product in acetone (40 mL) was added aqueous HCl (12 M, 20 mL), and the mixture was vigorously stirred at 0 °C for 10 s. Immediately, the mixture was poured into saturated aqueous $NaHCO_3$ (300 mL), and the resulting solution was extracted with AcOEt. The organic layer was washed with saturated aqueous $NaHCO_3$, brine, dried (Na_2SO_4) and evaporated. The residue was purified by silica gel column chromatography (5% AcOEt in hexane) to give **7** (2.27 g, 85%) as a colorless oil: $[\alpha]_D^{22}$ −12.0 (*c* 0.95, $CHCl_3$); ^1H-NMR (400 MHz, $CDCl_3$) δ 0.35 (1 H, m, cyclopropyl-CH_2), 0.52 (1 H, m, cyclopropyl-CH_2), 0.84 (1 H, m, cyclopropyl-CH), 0.91 (1 H, m, cyclopropyl-CH), 1.01 (9 H, s, *t*Bu), 2.27 (2 H, m, CH_2CHO), 3.49

(1 H, dd, J = 6.4, 10.7 Hz, CH_2OTBDPS), 3.69 (1 H, dd, J = 5.7, 10.7 Hz, CH_2OTBDPS), 7.35–7.44 (6 H, m, aromatic), 7.51–7.72 (4 H, m, aromatic), 9.75 (1 H, dd, J = 2.1, 2.3 Hz, C*H*O); ^{13}C-NMR (100 MHz, $CDCl_3$) δ 9.5, 10.2, 19.4, 20.5, 27.0, 47.6, 66.6, 127.5, 129.5, 133.7, 135.4, 201.9; LRMS (FAB) m/z 353 [(M+H)$^+$]; HRMS (FAB) calcd for $C_{22}H_{29}O_2Si$ 353.1937, found 353.1928 [(M+H)$^+$]; Found: C, 75.13; H, 8.05. Calc. for $C_{22}H_{28}O_2Si$: C, 74.95; H, 8.01%.

(2*R*,3*S*)-4-*tert*-Butyldiphenylsilyloxy-2,3-methanobutyraldehyde (*ent*-7)

Compound ***ent*-7** (2.41 g, 83%, colorless oil) was prepared from ***ent*-1**[6a] (2.80 g, 8.27 mmol) as described for the preparation of **7**: $[\alpha]_D^{22}$ +11.5 (c 0.98, $CHCl_3$); LRMS (FAB) m/z 353 [(M+H)$^+$]; HRMS (FAB) calcd for $C_{22}H_{29}O_2Si$ 353.1937, found 353.1925 [(M+H)$^+$]; Found: C, 75.02; H, 7.98. Calc. for $C_{22}H_{28}O_2Si$: C, 74.95; H, 8.01%. ^{1}H- and ^{13}C-NMR spectra were consistent with those of **7**.

(2*R*,3*R*)-4-*tert*-Butyldiphenylsilyloxy-2,3-methanobutyraldehyde (10)

Compound **10** (2.27 g, 92%, colorless oil) was prepared from **2**[6c] (2.37 g, 7.00 mmol) as described for the preparation of **7**: $[\alpha]_D^{24}$ −0.8 (c 1.15, $CHCl_3$); ^{1}H-NMR (400 MHz, $CDCl_3$) δ 0.05 (1 H, dd, J = 5.4, 10.6 Hz, cyclopropyl-CH_2), 0.77 (1 H, m, cyclopropyl-CH_2), 1.04 (9 H, s, *t*Bu), 1.08–1.26 (2 H, m, cyclopropyl-CH ×2), 2.32 (1 H, m, CH_2CHO), 2.51 (1 H, m, CH_2CHO), 3.43 (1 H, dd, J = 8.8, 11.3 Hz, CH_2OTBDPS), 3.89 (1 H, dd, J = 5.4, 11.3 Hz, CH_2OTBDPS), 7.35–7.43 (6 H, m, aromatic), 7.64–7.69 (4 H, m, aromatic), 9.83 (1 H, t, J = 1.8 Hz, C*H*O); ^{13}C-NMR (100 MHz, $CDCl_3$) δ 8.79, 9.30, 17.1, 19.2, 26.9, 42.9, 63.8, 127.6, 129.6, 133.6, 135.4, 135.5, 202.3; LRMS (FAB) m/z 353 [(M+H)$^+$]; HRMS (FAB) calcd for $C_{22}H_{29}O_2Si$ 353.1937, found 353.1938 [(M+H)$^+$]; Found: C, 74.90; H, 8.01. Calc. for $C_{22}H_{28}O_2Si$: C, 74.95; H, 8.01%.

(2*S*,3*S*)-4-*tert*-Butyldiphenylsilyloxy-2,3-methanobutyraldehyde (*ent*-10)

Compound ***ent*-10** (2.15 g, 80%, colorless oil) was prepared from ***ent*-2**[6c] (2.62 g, 7.68 mmol) as described for the preparation of **7**: $[\alpha]_D^{24}$ +0.14 (c 1.02, $CHCl_3$); LRMS (FAB) m/z 353 [(M+H)$^+$]; HRMS (FAB) calcd for $C_{22}H_{29}O_2Si$ 353.1937, found 353.1940 [(M+H)$^+$]; Found: C, 75.07; H, 8.11. Calc. for $C_{22}H_{28}O_2Si$: C, 74.95; H, 8.01%. ^{1}H- and ^{13}C-NMR spectra were consistent with those of **10**.

(2*S*,3*R*)-4-*tert*-Butyldiphenylsilyloxy-2,3-methano-1-(1-triphenylmethyl-1*H*-imidazol-4-yl)butane (8)

To a suspension of tosylmethyl isocyanide (667 mg, 3.43 mmol) and **7** (1.21 g, 3.43 mmol) in absolute EtOH (8 mL) was added sodium cyanide (17 mg, 0.34 mmol) at 0 °C, and the resulting mixture was stirred at the same temperature for 30 min. After the solvent was evaporated, the residue in a saturated solution of ammonia in absolute EtOH (60 mL) was heated at 120 °C in a steel tube for 24 h. After cooling, the solvent was evaporated, and the residue was co-evaporated with pyridine (×3). After drying the residue *in vacuo*, a solution of the residue and trityl chloride (954 mg, 3.43 mmol) in pyridine (10 mL) was stirred at room temperature for 12 h. After the solvent was evaporated, the residue was partitioned between AcOEt and aqueous HCl (1 M). The organic layer was washed with saturated aqueous $NaHCO_3$, brine, dried (Na_2SO_4), and evaporated. The residue was purified by silica gel column chromatography (20–50% AcOEt in hexane) to give **8** (1.03 g, 48%) as a colorless oil: $[\alpha]_D^{22}$ −18.7 (c 1.10, $CHCl_3$); ^{1}H-NMR (400 MHz, $CDCl_3$) δ 0.31–0.39 (2 H, m, cyclopropyl-CH_2), 0.81–0.90 (2 H, m, cyclopropyl-CH ×2), 1.02 (9 H, s, *t*Bu), 2.41 (1 H, dd, J = 6.8, 15.9 Hz, CH_2-imidazole), 2.59 (1 H, dd, J = 5.9, 15.9 Hz, CH_2-imidazole), 3.40 (1 H, dd, J = 6.3, 10.9 Hz, CH_2OTBDPS), 3.60 (1 H, dd, J = 5.4, 10.9 Hz, CH_2OTBDPS), 6.52 (1 H, s, imidazolyl) 7.11–7.13 (6 H, m, aromatic), 7.25–7.39 (16 H, m, aromatic & imidazolyl), 7.64–7.65 (4 H, m, aromatic); ^{13}C-NMR (100 MHz, $CDCl_3$) δ 9.86, 15.8, 19.2, 20.4, 26.8, 32.2, 67.0, 75.0, 117.8, 127.5, 127.9, 129.4, 129.7, 134.0, 135.6, 138.2, 141.4, 142.5; LRMS (FAB) m/z 633 [(M+H)$^+$]; HRMS (FAB) calcd for $C_{43}H_{45}N_2OSi$ 633.3301; found 633.3299 [(M+H)$^+$]; Found: C, 81.55; H, 7.05; N, 4.37. Calc. for $C_{43}H_{44}N_2OSi$: C, 81.60; H, 7.01; N, 4.43%.

(2*R*,3*S*)-4-*tert*-Butyldiphenylsilyloxy-2,3-methano-1-(1-triphenylmethyl-1*H*-imidazol-4-yl)butane (*ent*-8)

Compound ***ent*-8** (755 mg, 43%, colorless oil) was prepared from ***ent*-7** (970 mg, 2.75 mmol) as described for the preparation of **8**: $[\alpha]_D^{22}$ +18.3 (c 1.35, $CHCl_3$); LRMS (FAB) m/z 633 [(M+H)$^+$]; HRMS (FAB) calcd for $C_{43}H_{45}N_2OSi$ 633.3301; found 633.3300 [(M+H)$^+$]; Found: C, 81.38; H, 6.91; N, 4.60. Calc. for $C_{43}H_{44}N_2OSi$: C, 81.60; H, 7.01; N, 4.43%. ^{1}H- and ^{13}C-NMR spectra were consistent with those of **8**.

(2*R*,3*R*)-4-*tert*-Butyldiphenylsilyloxy-2,3-methano-1-(1-triphenylmethyl-1*H*-imidazol-4-yl)butane (11)

Compound **11** (744 mg, 51%, colorless oil) was prepared from **10** (821 mg, 2.33 mmol) as described for the preparation of **8**: $[\alpha]_D^{23}$ +4.9 (c 1.01, $CHCl_3$); ^{1}H-NMR (400 MHz, $CDCl_3$) δ 0.04 (1 H, m, cyclopropyl-CH_2), 0.66 (1 H, m, cyclopropyl-CH_2), 1.03 (9 H, s, *t*Bu), 1.07–1.18 (2 H, m, cyclopropyl-CH ×2), 2.39 (1 H, dd, J = 7.9, 15.8 Hz, CH_2-imidazole), 2.75 (1 H, dd, J = 5.4, 15.8 Hz, CH_2-imidazole), 3.68 (2 H, d, J = 6.7 Hz, CH_2OTBDPS), 6.51 (1 H, s, imidazolyl) 7.11–7.13 (6 H, m, aromatic), 7.26–7.39 (16 H, m, aromatic & imidazolyl), 7.64–7.68 (4 H, m, aromatic); ^{13}C-NMR (100 MHz, $CDCl_3$) δ 10.0, 15.6, 18.2, 19.5, 27.2, 28.0, 64.5, 75.3, 118.0, 127.8, 127.9, 128.2, 128.2, 129.7, 130.1, 134.4, 134.4, 135.9, 135.9, 138.6, 142.3, 142.9; LRMS (FAB) m/z 633 [(M+H)$^+$]; HRMS (FAB) calcd for $C_{43}H_{45}N_2OSi$ 633.3301; found 633.3300 [(M+H)$^+$]. Found: C, 81.84; H, 6.81; N, 4.21. Calc. for $C_{43}H_{44}N_2OSi$: C, 81.60; H, 7.01; N, 4.43%.

(2*S*,3*S*)-4-*tert*-Butyldiphenylsilyloxy-2,3-methano-1-(1-triphenylmethyl-1*H*-imidazol-4-yl)butane (*ent*-11)

Compound ***ent*-11** (922 mg, 58%, a colorless oil) was prepared from ***ent*-10** (890 mg, 2.52 mmol) as described for the preparation of **8**: $[\alpha]_D^{23}$ −4.6 (c 0.96, $CHCl_3$); LRMS (FAB) m/z 633 [(M+H)$^+$]; HRMS (FAB) calcd for $C_{43}H_{45}N_2OSi$ 633.3301; found 633.3310 [(M+H)$^+$]; Found: C, 81.77; H, 6.89; N, 4.18. Calc. for

$C_{43}H_{44}N_2OSi$: C, 81.60; H, 7.01; N, 4.43%. ^{1}H- and ^{13}C-NMR spectra were consistent with those of **11**.

(2*S*,3*R*)-4-Formyl-2,3-methano-1-(1-triphenylmethyl-1*H*-imidazol-4-yl)butane (9)

A mixture of **8** (633 mg, 1.00 mmol) and TBAF (1.0 M THF, 2.0 mL, 2.0 mmol) in THF (6 mL) was stirred at room temperature for 12 h. After the solvent was evaporated, the residue was purified by silica gel column chromatography (50% AcOEt in hexane then 3% MeOH in $CHCl_3$) to give an alcohol product. To a solution of the alcohol in CH_2Cl_2 (10 mL) was added Dess–Martin periodinane (509 mg, 1.20 mmol), and the resulting mixture was stirred at room temperature for 2 h. After addition of saturated aqueous $Na_2S_2O_3$/$NaHCO_3$ (1 : 3), the resulting mixture was stirred vigorously for 10 min. The mixture was extracted with AcOEt, and the organic layer was washed with saturated aqueous $NaHCO_3$, brine, dried (Na_2SO_4), and evaporated. The residue was purified by silica gel column chromatography (33% AcOEt in hexane) to give **9** (305 mg, 78%) as a light brown amorphous solid: $[\alpha]_D^{24}$ −26.0 (*c* 1.00, $CHCl_3$); ^{1}H-NMR (400 MHz, $CDCl_3$) δ 1.04 (1 H, m, cyclopropyl-CH_2), 1.32 (1 H, m, cyclopropyl-CH_2), 1.68–1.83 (2 H, m, cyclopropyl-CH ×2), 2.66 (2 H, d, J = 6.3 Hz, CH_2-imidazole), 6.57 (1 H, s, imidazolyl) 7.12–7.15 (6 H, m, aromatic), 7.32–7.36 (10 H, m, aromatic & imidazolyl), 9.01 (1 H, d, J = 5.3 Hz, C*H*O); ^{13}C-NMR (100 MHz, $CDCl_3$) δ 12.8, 24.2, 27.2, 27.7, 75.1, 117.9, 127.9, 129.6, 138.4, 140.3, 142.5, 201.9; LRMS (EI) *m*/*z* 392 (M^+); HRMS (EI) calcd for $C_{27}H_{24}N_2O$ 392.1889; found 392.1880 (M^+); Found: C, 82.77; H, 6.39; N, 7.18. Calc. for $C_{27}H_{24}N_2O$: C, 82.62; H, 6.16; N, 7.14%.

(2*R*,3*S*)-4-Formyl-2,3-methano-1-(1-triphenylmethyl-1*H*-imidazol-4-yl)butane (*ent*-9)

Compound ***ent*-9** (305 mg, 78%, white amorphous solid) was prepared from ***ent*-8** (633 mg, 1.00 mmol) as described for the preparation of **9**: $[\alpha]_D^{24}$ +25.2 (*c* 1.00, $CHCl_3$); LRMS (EI) *m*/*z* 392 (M^+); HRMS (EI) calcd for $C_{27}H_{24}N_2O$ 392.1889; found 392.1890 (M^+); Found: C, 82.83; H, 6.23; N, 7.42. Calc. for $C_{27}H_{24}N_2O$: C, 82.62; H, 6.16; N, 7.14%. ^{1}H- and ^{13}C-NMR spectra were consistent with those of **9**.

(2*R*,3*R*)-4-Formyl-2,3-methano-1-(1-triphenylmethyl-1*H*-imidazol-4-yl)butane (12)

Compound **12** (259 mg, 65%, white amorphous solid) was prepared from **11** (637 mg, 1.01 mmol) as described for the preparation of **9**: $[\alpha]_D^{23}$ −24.5 (*c* 1.00, $CHCl_3$); ^{1}H-NMR (400 MHz, $CDCl_3$) δ 1.25–1.34 (2 H, m, cyclopropyl-CH_2), 1.83–1.97 (2 H, m, cyclopropyl-CH ×2), 2.67 (1 H, dd, J = 8.2, 15.5 Hz, CH_2-imidazole), 2.95 (1 H, dd, J = 6.3, 15.5 Hz, CH_2-imidazole), 6.53 (1 H, s, imidazolyl) 7.10–7.15 (6 H, m, aromatic), 7.31–7.34 (9 H, m, aromatic), 7.36 (1 H, s, imidazolyl), 9.38 (1 H, d, J = 5.0 Hz, C*H*O); ^{13}C-NMR (100 MHz, $CDCl_3$) δ 15.0, 24.2, 27.2, 27.7, 75.1, 117.9, 127.8, 129.6, 138.4, 140.3, 142.2, 200.9; LRMS (EI) *m*/*z* 392 (M^+); HRMS (EI) calcd for $C_{27}H_{24}N_2O$ 392.1889; found 392.1890 (M^+); Found: C, 82.91; H, 6.00; N, 6.95. Calc. for $C_{27}H_{24}N_2O$: C, 82.62; H, 6.16; N, 7.14%.

(2*S*,3*S*)-4-Formyl-2,3-methano-1-(1-triphenylmethyl-1*H*-imidazol-4-yl)butane (*ent*-12)

Compound ***ent*-12** (290 mg, 65%, a white solid) was prepared from ***ent*-11** (720 mg, 1.14 mmol) as described for the preparation of **9**: $[\alpha]_D^{22}$ +25.0 (*c* 1.05, $CHCl_3$); LRMS (EI) *m*/*z* 392 (M^+); HRMS (EI) calcd for $C_{27}H_{24}N_2O$ 392.1889; found 392.1888 (M^+); Found: C, 82.78; H, 5.97; N, 6.90. Calc. for $C_{27}H_{24}N_2O$: C, 82.62; H, 6.16; N, 7.14%. ^{1}H- and ^{13}C-NMR spectra were consistent with those of **12**.

(2*S*,3*R*)-*trans*-4-(4-Chlorobenzylamino)-2,3-methano-1-(1*H*-imidazol-4-yl)butane (5b)

A mixture of **9** (48 mg, 0.12 mmol), 4-chlorobenzylamine (98%, 16 μL, 0.13 mmol) and 2-picoline borane (13 mg, 0.13 mmol) in MeOH/AcOH (10 : 1, 1.1 mL) was stirred at room temperature for 8 h. After the addition of aqueous HCl (1 M, 1 mL), the mixture was stirred at 0 °C for 10 min and then the solvent was evaporated. The residue was partitioned between Et_2O and aqueous NaOH (2 M), and the organic layer was washed with H_2O, brine, dried (Na_2SO_4), and evaporated. The residue was purified by neutral silica gel column chromatography (10–20% MeOH in $CHCl_3$) to give the crude amine product. A solution of the amine, trityl chloride (56 mg, 0.20 mmol) and Et_3N (28 μL, 0.20 mmol) in CH_2Cl_2 (1 mL) was stirred at room temperature for 12 h. After addition of MeOH (1 mL), the solvent was evaporated. The residue was partitioned between Et_2O and aqueous HCl (0.5 M), and the organic layer was washed with saturated aqueous $NaHCO_3$ and brine, dried (Na_2SO_4), and evaporated. The residue was purified by neutral silica gel column chromatography (17–33% AcOEt in hexane) to give the amine as an amorphous solid. A solution of the amine in EtOH (2.0 mL)/aqueous HCl (4 M, 1.0 mL) was stirred at 78 °C for 2 h, and then the solvent was evaporated. The residue was partitioned between aqueous HCl (1 M) and CH_2Cl_2, and the aqueous layer was neutralized with aqueous NaOH (2 M). The resulting solution was extracted with Et_2O (×3), and the organic layer was washed with H_2O and brine, dried (Na_2SO_4), and evaporated. The residue was purified by Iatron beads column chromatography (0–100% MeOH in $CHCl_3$) to give **5b** (10 mg, 30%, colorless amorphous solid) as a free amine: ^{1}H-NMR (500 MHz, $CDCl_3$) δ 0.47–0.54 (2 H, m, cyclopropyl-CH_2), 0.79–0.86 (2 H, m, cyclopropyl-CH ×2), 2.10–2.17 (2 H, m, CH_2-imidazole), 3.02–3.09 (2 H, m, CH_2NH), 3.75 (1 H, d, J = 13.2 Hz, benzyl-CH_2), 3.84 (1 H, d, J = 13.2 Hz, benzyl-CH_2), 6.77 (1 H, s, imidazolyl), 7.25–7.26 (2 H, m, aromatic), 7.30–7.32 (2 H, m, aromatic) 7.36 (1 H, s, imidazolyl); ^{13}C-NMR (125 MHz, $CDCl_3$) δ 10.2, 17.2, 19.2, 29.3, 53.0, 53.4, 120.9, 128.7, 128.7, 129.6, 129.6, 133.1, 133.1, 134.1, 137.5; LRMS (EI) *m*/*z* 275 (M^+); HRMS (EI) calcd for $C_{15}H_{18}ClN_3$ 275.1189, found 275.1190 (M^+); Found: C, 65.03; H, 6.63; N, 15.49. Calc. for $C_{15}H_{18}ClN_3$: C, 65.33; H, 6.58; N, 15.24%; The free amine **5b** was dissolved in aqueous HCl (4 M), and the solvent was evaporated. The residue was triturated with Et_2O to give **5b dihydrochloride** (12 mg) as a white amorphous solid: $[\alpha]_D^{22}$ −25.2 (*c* 1.01, MeOH); ^{1}H-NMR (400 MHz, CD_3OD) δ 0.76 (2 H, m, cyclopropyl-CH_2), 1.18 (1 H, m, cyclopropyl-CH), 1.24 (1 H, m, cyclopropyl-CH), 2.58 (1 H, dd, J = 7.7, 14.5 Hz, CH_2-imidazole), 2.91–2.96 (2 H, m, CH_2NH), 3.14 (1 H, dd, J = 6.8, 14.5 Hz, CH_2-imidazole), 4.22 (2 H, s, benzyl-CH_2), 7.42 (1 H,

s, imidazolyl), 7.47 (2 H, d, J = 8.2 Hz, aromatic), 7.55 (2 H, d, J = 8.2 Hz, aromatic), 8.83 (1 H, s, imidazolyl); LRMS (EI) m/z 275 [(M–2HCl)$^+$]; HRMS (EI) calcd for $C_{15}H_{18}ClN_3$ 275.1189, found 275.1189 [(M–2HCl)$^+$]; Found: C, 51.52; H, 5.86; N, 11.78. Calc. for $C_{15}H_{20}Cl_3N_3$: C, 51.67; H, 5.78; N, 12.05%.

(2*R*,3*S*)-*trans*-4-(4-Chlorobenzylamino)-2,3-methano-1-(1*H*-imidazol-4-yl)butane (*ent*-5b)

Compound ***ent*-5b** (18 mg, 60%, colorless amorphous solid) was prepared from ***ent*-9** (45 mg, 0.12 mmol) as described for the preparation of **5b**: LRMS (EI) m/z 275 (M$^+$); HRMS (EI) calcd for $C_{15}H_{18}ClN_3$ 275.1189, found 275.1185 (M$^+$); Found: C, 65.00; H, 6.79; N, 15.52. Calc. for $C_{15}H_{18}ClN_3$: C, 65.33; H, 6.58; N, 15.24%; ^{1}H- and ^{13}C-NMR spectra were consistent with those of **5b**; The free amine ***ent*-5b** was dissolved in aqueous HCl (4 M), and the solvent was then evaporated. The residue was triturated with Et_2O to give ***ent*-5b dihydrochloride** (20 mg) as a white amorphous solid: $[\alpha]_D^{22}$ +24.6 (c 1.10, MeOH); LRMS (EI) m/z 275 [(M–2HCl)$^+$]; HRMS (EI) calcd for $C_{15}H_{18}ClN_3$ 275.1189, found 275.1191 [(M–2HCl)$^+$]; Found: C, 51.39; H, 5.98; N, 11.81. Calc. for $C_{15}H_{20}Cl_3N_3$: C, 51.67; H, 5.78; N, 12.05%. ^{1}H-NMR spectrum was consistent with that of **5b dihydrochloride**.

(2*R*,3*R*)-*cis*-4-(4-Chlorobenzylamino)-2,3-methano-1-(1*H*-imidazol-4-yl)butane (6b)

Compound **6b** (27 mg, 49%, colorless amorphous solid) was prepared from **12** (78 mg, 0.20 mmol) as described for the preparation of **5b**: ^{1}H-NMR (500 MHz, $CDCl_3$) δ 0.81 (1 H, dd, J = 5.7, 10.9 Hz, cyclopropyl-CH_2), 0.87 (1 H, m, cyclopropyl-CH_2), 1.02-1.10 (2 H, m, cyclopropyl-CH ×2), 2.08 (1 H, dd, J = 4.6, 15.5 Hz, CH_2-imidazole), 2.40 (1 H, t, J = 12.6 Hz, CH_2NH), 3.15 (1 H, dd, J = 2.3, 15.5 Hz, CH_2-imidazole), 3.34 (1 H, dd, J = 2.9, 12.6 Hz, CH_2NH), 3.78 (1 H, d, J = 12.6 Hz, benzyl-CH_2), 3.93 (1 H, d, J = 12.6 Hz, benzyl-CH_2), 6.76 (1 H, s, imidazolyl), 7.26 (1 H, s, imidazolyl), 7.30 (2 H, d, J = 8.6 Hz, aromatic), 7.35 (2 H, d, J = 8.6 Hz, aromatic); ^{13}C-NMR (125 MHz, $CDCl_3$) δ 8.47, 15.3, 17.1, 24.4, 48.1, 53.0, 123.3, 128.9, 128.9, 129.7, 129.7, 131.3, 133.5, 134.8, 136.9; LRMS (EI) m/z 275 (M$^+$); HRMS (EI) calcd for $C_{15}H_{18}ClN_3$ 275.1189, found 275.1187 (M$^+$); Found: C, 65.10; H, 6.88; N, 14.93. Calc. for $C_{15}H_{18}ClN_3$: C, 65.33; H, 6.58; N, 15.24%; The free amine **6b** was dissolved in aqueous HCl (4 M), and the solvent was then evaporated. The residue was triturated with Et_2O to give **6b dihydrochloride** (30 mg) as a white solid: $[\alpha]_D^{22}$ –11.1 (c 0.96, MeOH); ^{1}H-NMR (400 MHz, CD_3OD) δ 0.56 (1 H, ddd, J = 5.4, 5.9, 11.3 Hz, cyclopropyl-CH_2), 1.06 (1 H, ddd, J = 8.6, 11.3, 12.6 Hz, cyclopropyl-CH_2), 1.36 (1 H, m, cyclopropyl-CH), 1.43 (1 H, m, cyclopropyl-CH), 2.74 (1 H, dd, J = 8.6, 16.3 Hz, CH_2-imidazole), 2.97 (1 H, dd, J = 6.3, 16.3 Hz, CH_2-imidazole), 3.05 (1 H, dd, J = 3.6, 12.7 Hz, CH_2NH), 3.41 (1 H, dd, J = 5.4, 12.7 Hz, CH_2NH), 4.24 (1 H, d, J = 13.1 Hz, benzyl-CH_2), 4.30 (1 H, d, J = 13.1 Hz, benzyl-CH_2), 7.44 (1 H, d, J = 1.1 Hz, imidazolyl), 7.48 (2 H, d, J = 8.6 Hz, aromatic), 7.58 (2 H, d, J = 8.6 Hz, aromatic), 8.84 (1 H, d, J = 1.1 Hz, imidazolyl); LRMS (EI) m/z 275 [(M–2HCl)$^+$]; HRMS (EI) calcd for $C_{15}H_{18}ClN_3$ 275.1189, found 275.1192 [(M–2HCl)$^+$]; Found: C, 51.42; H, 5.95; N, 11.88. Calc. for $C_{15}H_{20}Cl_3N_3$: C, 51.67; H, 5.78; N, 12.05%.

(2*S*,3*S*)-*cis*-4-(4-Chlorobenzylamino)-2,3-methano-1-(1*H*-imidazol-4-yl)butane (*ent*-6b)

Compound ***ent*-6b** (20 mg, 43%, white amorphous solid) was prepared from ***ent*-12** (69 mg, 0.17 mmol) as described for the preparation of **5b**; LRMS (EI) m/z 275 (M$^+$); HRMS (EI) calcd for $C_{15}H_{18}ClN_3$ 275.1189, found 275.1167 (M$^+$); Found: C, 65.14; H, 6.76; N, 15.00. Calc. for $C_{15}H_{18}ClN_3$: C, 65.33; H, 6.58; N, 15.24%; ^{1}H- and ^{13}C-NMR spectra were consistent with those of **6b**; The free amine ***ent*-6b** was dissolved in aqueous HCl (4 M), and the solvent was then evaporated. The residue was triturated with Et_2O to give ***ent*-6b dihydrochloride** (22 mg) as a white solid: $[\alpha]_D^{22}$ +10.8 (c 0.90, MeOH); LRMS (EI) m/z 275 [(M–2HCl)$^+$]; HRMS (EI) calcd for $C_{15}H_{18}ClN_3$ 275.1189, found 275.1188 [(M–2HCl)$^+$]; Found: C, 51.55; H, 5.96; N, 12.13. Calc. for $C_{15}H_{20}Cl_3N_3$: C, 51.67; H, 5.78; N, 12.05%. ^{1}H-NMR spectrum was consistent with that of **6b dihydrochloride**.

(2*S*,3*R*)-*trans*-4-Amino-2,3-methano-1-(1*H*-imidazol-4-yl)butane (5a)

A mixture of **9** (136 mg, 0.347 mmol), (±)-*tert*-butanesulfinamide (59 mg, 0.49 mmol) and anhydrous $CuSO_4$ (560 mg, 3.47 mmol) in CH_2Cl_2 (3 mL) was stirred at room temperature for 24 h. After filtration of the reaction mixture with Celite, the filtrate was evaporated, and the residue was partitioned between $CHCl_3$ and cold aqueous HCl (0.5 M). The organic layer was washed with H_2O and brine, dried (Na_2SO_4), and evaporated. A solution of the residue and added $NaBH_4$ (17 mg, 0.46 mmol) in MeOH (3 mL) was stirred at 0 °C for 2 h. After the solvent was evaporated, the residue was purified by silica gel column chromatography (0–2% MeOH in $CHCl_3$) to give **13** (120 mg, diastereomixture) as a colorless amorphous solid. A mixture of **13** (99 mg) and an EtOH solution of HCl (1 M, 3.0 mL) was stirred at 78 °C for 3 h. After the mixture was evaporated, the residue was washed with Et_2O. The residue was purified by NH silica gel column chromatography (0–20% MeOH in $CHCl_3$) to give **5a** (21 mg, 50% for three steps, colorless amorphous solid) as a free amine: ^{1}H-NMR (500 MHz, CD_3OD) δ 0.41 (2 H, m, cyclopropyl-CH_2), 0.80 (1 H, m, cyclopropyl-CH), 0.87 (1 H, m, cyclopropyl-CH), 2.45–2.55 (4 H, m, CH_2-imidazole & CH_2NH_2), 6.78 (1 H, s, imidazolyl), 7.52 (1 H, s, imidazolyl); ^{13}C-NMR (125 MHz, CD_3OD) δ 11.0, 18.2, 21.0, 31.2, 46.2, 117.8, 135.6, 137.4; LRMS (EI) m/z 151 (M$^+$); HRMS (EI) calcd for $C_8H_{13}N_3$ 151.1110, found 151.1100 (M$^+$); Found: C, 63.11; H, 8.89; N, 27.59. Calc. for $C_8H_{13}N_3$: C, 63.54; H, 8.67; N, 27.79%; The free amine **5a** was dissolved in aqueous HCl (4 M), and the solvent was then evaporated. The residue was triturated with Et_2O to give **5a dihydrochloride** (20 mg) as a white amorphous solid: $[\alpha]_D^{22}$ –44.1 (c 1.10, MeOH); ^{1}H-NMR (400 MHz, CD_3OD) δ 0.72 (2 H, m, cyclopropyl-CH_2), 1.12 (1 H, m, cyclopropyl-CH), 1.19 (1 H, m, cyclopropyl-CH), 2.58 (1 H, dd, J = 8.2, 15.9 Hz, CH_2-imidazole), 2.78 (1 H, dd, J = 7.7, 13.1 Hz, CH_2NH_2), 2.92 (1 H, dd, J = 6.3, 15.9 Hz, CH_2-imidazole), 2.99 (1 H, dd, J = 7.2, 13.1 Hz, CH_2NH_2), 7.42 (1 H, s, imidazolyl), 8.84 (1 H, s, imidazolyl); LRMS (EI) m/z 151 [(M–2HCl)$^+$]; HRMS (EI) calcd for $C_8H_{13}N_3$ 151.1110, found 151.1102 [(M–2HCl)$^+$]; Found: C, 41.50; H, 6.93; N, 17.99. Calc. for $C_8H_{15}Cl_2N_3 \cdot 0.5H_2O$: C, 41.21; H, 6.92; N, 18.02%.

(2*R*,3*S*)-*trans*-4-Amino-2,3-methano-1-(1*H*-imidazol-4-yl)butane (*ent*-5a)

Compound ***ent*-5a** (23 mg, 61% for three steps, colorless amorphous solid) was prepared from ***ent*-9** (99 mg, 0.25 mmol) as described for the preparation of **5a**: LRMS (EI) *m/z* 151 (M^+); HRMS (EI) calcd for $C_8H_{13}N_3$ 151.1110, found 151.1121 (M^+); Found: C, 63.20; H, 8.98; N, 27.48. Calc. for $C_8H_{13}N_3$: C, 63.54; H, 8.67; N, 27.79%; ^{1}H- and ^{13}C-NMR spectra were consistent with those of **5a**; The free amine ***ent*-5a** was dissolved in aqueous HCl (4 M), and the solvent was then evaporated. The residue was triturated with Et_2O to give ***ent*-5a dihydrochloride** (25 mg) as a white amorphous solid: $[\alpha]_D^{22}$ +44.9 (*c* 1.12, MeOH); LRMS (EI) *m/z* 151 [(M–2HCl)$^+$]; HRMS (EI) calcd for $C_8H_{13}N_3$ 151.1110, found 151.1099 [(M–2HCl)$^+$]; Found: C, 42.49; H, 6.82; N, 18.35. Calc. for $C_8H_{15}Cl_2N_3 \cdot 0.1H_2O$: C, 42.53; H, 6.78; N, 18.60%. ^{1}H-NMR spectrum was consistent with that of **5a dihydrochloride**.

(2*R*,3*R*)-*cis*-4-Amino-2,3-methano-1-(1*H*-imidazol-4-yl)butane (6a)

Compound **6a** (18 mg, 59% for three steps, colorless amorphous solid) was prepared from **12** (79 mg, 0.20 mmol) as described for the preparation of **5a**: ^{1}H-NMR (500 MHz, CD_3OD) δ 0.18 (1 H, dd, J = 5.2, 10.9 Hz, cyclopropyl-CH_2), 0.84 (1 H, m, cyclopropyl-CH_2), 1.08–1.19 (2 H, m, cyclopropyl-CH ×2), 2.42 (1 H, dd, J = 8.6, 15.4 Hz, CH_2-imidazole), 2.75 (1 H, dd, J = 9.2, 13.5 Hz, CH_2NH$_2$), 2.87 (1 H, dd, J = 5.2, 15.4 Hz, CH_2-imidazole), 3.05 (1 H, dd, J = 5.7, 13.5 Hz, CH_2NH$_2$), 6.87 (1 H, s, imidazolyl), 7.61 (1 H, d, J = 1.1 Hz, imidazolyl); ^{13}C-NMR (125 MHz, CD_3OD) δ 10.1, 17.1, 18.3, 26.6, 41.6, 117.4, 135.8, 138.4; LRMS (EI) *m/z* 151 (M^+); HRMS (EI) calcd for $C_8H_{13}N_3$ 151.1110, found 151.1109 (M^+); Found: C, 63.11; H, 8.89; N, 27.59. Calc. for $C_8H_{13}N_3$: C, 63.54; H, 8.67; N, 27.79%; The free amine **6a** was dissolved in aqueous HCl (4 M), and the solvent was then evaporated. The residue was triturated with Et_2O to give **6a dihydrochloride** (20 mg) as a white amorphous solid: $[\alpha]_D^{22}$ +2.3 (*c* 0.66, MeOH); ^{1}H-NMR (500 MHz, CD_3OD) δ 0.45 (1 H, dd, J = 5.4, 11.3 Hz, cyclopropyl-CH_2), 1.02 (1 H, m, cyclopropyl-CH_2), 1.31 (1 H, m, cyclopropyl-CH), 1.41 (1 H, m, cyclopropyl-CH), 2.71 (1 H, dd, J = 8.6, 16.3 Hz, CH_2-imidazole), 2.88 (1 H, dd, J = 9.0, 13.1 Hz, CH_2NH$_2$), 3.00 (1 H, dd, J = 6.3, 16.3 Hz, CH_2-imidazole), 3.25 (1 H, dd, J = 5.9, 13.1 Hz, CH_2NH$_2$), 7.44 (1 H, d, J = 0.9 Hz, imidazolyl), 8.86 (1 H, d, J = 1.4 Hz, imidazolyl); LRMS (EI) *m/z* 151 [(M–2HCl)$^+$]; HRMS (EI) calcd for $C_8H_{13}N_3$ 151.1110, found 151.1097 [(M–2HCl)$^+$]; Found: C, 42.60; H, 6.88; N, 18.65. Calc. for $C_8H_{15}Cl_2N_3$: C, 42.87; H, 6.75; N, 18.75%.

(2*S*,3*S*)-*cis*-4-Amino-2,3-methano-1-(1*H*-imidazol-4-yl)butane (*ent*-6a)

Compound ***ent*-6a** (20 mg, 39% for three steps, colorless amorphous solid) was prepared from ***ent*-12** (131 mg, 0.334 mmol) as described for the preparation of **5a**: LRMS (EI) *m/z* 151 (M^+); HRMS (EI) calcd for $C_8H_{13}N_3$ 151.1110, found 151.1095 (M^+); Found: C, 63.39; H, 9.02; N, 27.36. Calc. for $C_8H_{13}N_3$: C, 63.54; H, 8.67; N, 27.79%; ^{1}H- and ^{13}C-NMR spectrum was consistent with that of **6a**; The free amine ***ent*-6a** was dissolved in aqueous HCl (4 M), and the solvent was then evaporated. The residue was triturated with Et_2O to give ***ent*-6a dihydrochloride** (22 mg) as a white solid: $[\alpha]_D^{22}$ –2.2 (*c* 0.58, MeOH); LRMS (EI) *m/z* 151 [(M–2HCl)$^+$]; HRMS (EI) calcd for $C_8H_{13}N_3$ 151.1110, found 151.1121 [(M–2HCl)$^+$]; Found: C, 41.31; H, 6.95; N, 17.93. Calc. for $C_8H_{15}Cl_2N_3 \cdot 0.5H_2O$: C, 41.21; H, 6.92; N, 18.02%. ^{1}H-NMR spectrum was consistent with that of **6a dihydrochloride**.

Binding assay with human histamine receptors

The assay was performed according to the method described previously.[6c] The dihydrochloride salts of the final compounds were used in the assay.

Luciferase reporter gene assay

The assay was performed according to the method described previously.[6b] Briefly, 3 × 10^4 cells of 293-EBNA (Invitrogen) were harvested on collagen-coated 48-well plates for 24 h. An expression plasmid for $G_{\alpha q/i}$, chimera G_α protein of $G_{\alpha q}$ and $G_{\alpha i}$, was constructed and cotransfected with an H_3- or H_4-expression plasmid and a pSRE-Luc. The following day, the cells were treated with histamine (10^{-5} or 10^{-6} M) and/or each compound (10^{-5} M) for 5 h, and laid on ice. Intracellular luciferase activity in aliquots from each lysate was measured using a model ML3000 luminometer (Dynatech Laboratories). The dihydrochloride salts of the final compounds were used in the assay.

Docking simulation

Using the homology modeling of the H_3 receptor that was constructed previously,[6d] the docking simulation was performed according to the method described previously.[6d]

Acknowledgements

This investigation was supported by a Grant-in-Aids for Scientific Research (21390028) from the Japan Society for the Promotion of Science. We are grateful to Sanyo Fine Co., Ltd. for the gift of the chiral epichlorohydrins.

References

1 (*a*) J.-M. Arrang, M. Garbarg and J.-C. Schwartz, *Nature*, 1983, **302**, 832–837; (*b*) *The Histamine H_3 Receptor: A Target for New Drugs*, ed. R. Leurs and H. Timmerman, Elsevier, Amsterdam, 1998; (*c*) R. Leurs, R. A. Bakker, H. Timmerman and I. J. P. de Esch, *Nat. Rev. Drug Discovery*, 2005, **4**, 107–120; (*d*) S. Celanire, M. Wijtmans, P. Talaga, R. Leurs and I. J. P. de Esch, *Drug Discovery Today*, 2005, **10**, 1613–1627; (*e*) T. A. Esbenshade, G. B. Fox and M. D. Cowart, *Mol. Interventions*, 2006, **6**, 77–88.

2 (*a*) M. Krause, H. Stark, and W. Schunack, Medicinal chemistry of histamine H_3 receptor agonists, pp. 175–196. In ref. 1b; (*b*) K. Onodera, and T. Watanabe, Histamine H_3 antagonists as potential therapeutics in the CNS, pp. 255–268. In ref. 1b.

3 (*a*) P. Ling, K. Ngo, S. Nguyen, R. L. Thurmond, J. P. Edwards, L. Karlsson and W. P. Fung-Leung, *Pharmacol.*, 2004, **142**, 161–171; (*b*) W. P. Fung-Leung, R. L. Thurmond, P. Ling and L. Karlsson, *Curr. Opin. Investig. Drugs*, 2004, **11**, 1174–1183; (*c*) H. D. Lim, R. M. van Rijn, P. Ling, R. L. Thurmond, R. A. Bakker and R. Leurs, *J. Pharmacol. Exp. Ther.*, 2005, **314**, 1310–1321.

4 (*a*) T. Klabunde and G. Hessler, *ChemBioChem*, 2002, **3**, 928–944; (*b*) K. Palczewski, T. Kumasaka, T. Hori, C. A. Behnke, H. Motoshima, B. A. Fox, I. Le Trong, D. C. Teller, T. Okada, R. E. Stenkamp, M. Yamamoto and M. Miyano, *Science*, 2000, **289**, 739–745; (*c*) V. Sarramegna, F. Talmont, P. Demange and A. Milon, *Cell. Mol. Life Sci.*, 2003, **60**, 1529–1546; (*d*) S. Schlyer and R. Horuk, *Drug Discovery Today*, 2006, **11**, 481–493; and references therein.

5 Recently, several X-ray crystallographic analyses of GPCR have been reported: (*a*) V. Cherezov, D. M. Rosenbaum, M. A. Hanson, S. G. Rasmussen, F. S. Thian, T. S. Kobilka, H. J. Choi, P. Kuhn, W. I. Weis, B. K. Kobilka and R. C. Stevens, *Science*, 2007, **318**, 1258–1265; (*b*) D. M. Rosenbaum, V. Cherezov, M. A. Hanson, S. G. Rasmussen, F. S. Thian, T. S. Kobilka, H. J. Choi, X. J. Yao, W. I. Weis, R. C. Stevens and B. K. Kobilka, *Science*, 2007, **318**, 1266–1273; (*c*) S. G. Rasmussen, H. J. Choi, D. M. Rosenbaum, T. S. Kobilka, F. S. Thian, P. C. Edwards, M. Burghammer, V. R. Ratnala, R. Sanishvili, R. F. Fischetti, G. F. Schertler, W. I. Weis and B. K. Kobilka, *Nature*, 2007, **450**, 383–387.

6 (*a*) Y. Kazuta, A. Matsuda and S. Shuto, *J. Org. Chem.*, 2002, **67**, 1669–1677; (*b*) Y. Kazuta, K. Hirano, K. Natsume, S. Yamada, R. Kimura, S. Matsumoto, K. Furuichi, A. Matsuda and S. Shuto, *J. Med. Chem.*, 2003, **46**, 1980–1988; (*c*) M. Watanabe, Y. Kazuta, H. Hayashi, S. Yamada, A. Matsuda and S. Shuto, *J. Med. Chem.*, 2006, **49**, 5787–5796; (*d*) M. Watanabe, T. Hirokawa, T. Kobayashi, A. Yoshida, Y. Ito, S. Yamada, N. Orimoto, Y. Yamasaki, M. Arisawa and S. Shuto, *J. Med. Chem.*, 2010, **53**, 3585–3593.

7 The cyclopropane-based stereochemical diversity-oriented strategy was also effectively used for identifying potent proteasome inhibitors: (*a*) K. Yoshida, K. Yamaguchi, T. Sone, Y. Unno, A. Asai, H. Yokosawa, A. Matsuda, M. Arisawa and S. Shuto, *Org. Lett.*, 2008, **10**, 3571–3574; (*b*) K. Yoshida, K. Yamaguchi, A. Mizuno, Y. Unno, A. Asai, T. Sone, H. Yokosawa, A. Matsuda, M. Arisawa and S. Shuto, *Org. Biomol. Chem.*, 2009, **7**, 1868–1877.

8 For examples of the cyclopropane-based conformational restriction, see the following: (*a*) P. D. Armstrong, G. J. Cannon and J. P. Long, *Nature*, 1968, **220**, 65–66; (*b*) K. Shimamoto and Y. Ofune, *J. Med. Chem.*, 1996, **39**, 407–423; (*c*) S. H. Stammer, *Tetrahedron*, 1990, **46**, 2231–2254; (*d*) S. F. Martin, M. P. Dwyer, B. Hartmann and K. S. Knight, *J. Org. Chem.*, 2000, **65**, 1305–1318; (*e*) T. Sekiyama, S. Hatsuya, Y. Tanaka, M. Uchiyama, N. Ono, S. Iwayama, M. Oikawa, K. Suzuki, M. Okunishi and T. Tsuji, *J. Med. Chem.*, 1998, **41**, 1284–1298.

9 (*a*) H. N. C. Wong, M.-Y. Hon, C.-Y. Tse and Y.-C. Yip, *Chem. Rev.*, 1989, **89**, 165–198; (*b*) V. K. Singh, A. DattaGupta and G. Sekar, *Synthesis*, 1997, 137–149; (*c*) M. P. Doyle and M. N. Protopopova, *Tetrahedron*, 1998, **54**, 7919–7946; (*d*) J. Cossy, N. Blanchard and C. Meyer, *Synthesis*, 1999, 1063–1075; (*e*) *Small Ring Compounds in Organic Synthesis VI. Topic in Current Chemistry 207*, A. de Meijere, Ed.; Springer: Berlin, 1999; (*f*) H. Lebel, J.-F. Marcoux, C. Molinaro and A. B. Charette, *Chem. Rev.*, 2003, **103**, 977–1050; (*g*) P. Garcia, D. Diez, A. B. Anton, N. M. Garrido, I. S. Marcos, P. Basabe and J. G. Urones, *Mini-Rev. Org. Chem.*, 2006, **3**, 291–314; (*h*) P. Muller, Y. ves F. Allenbach, S. Chappellet and A Ghanem, *Synthesis*, 2006, **10**, 1689–1696.

10 D. A. Horne, K. Yakushijin and G. A. Buchi, *Heterocycles*, 1994, **39**, 3957–3960.

11 (*a*) R. Kitbunnadaj, O. P. Zuiderveld, I. J. P. de Esch, R. C. Vollinga, R. Bakker, M. Lutz, A. L. Spek, E. Cavoy, M.-F. Deltent, W. M. P. B. Menge, H. Timmerman and R. Leurs, *J. Med. Chem.*, 2003, **46**, 5445–5457; (*b*) R. Kitbunnadaj, M. Hoffmann, S. A. Fratantoni, G. Bongers, R. A. Bakker, K. Wieland, A. el Jilali, I. J. P. de Esch, W. M. P. B. Menge, H. Timmerman and R. Leurs, *Bioorg. Med. Chem.*, 2005, **13**, 6309–6323.

12 An example of an H_3 receptor antagonist having a primary amino function without a hydrophobic group: R. C. Vollinga, W. M. P. B. Menge, R. Leurs and H. Timmerman, *J. Med. Chem.*, 1995, **38**, 266–271.